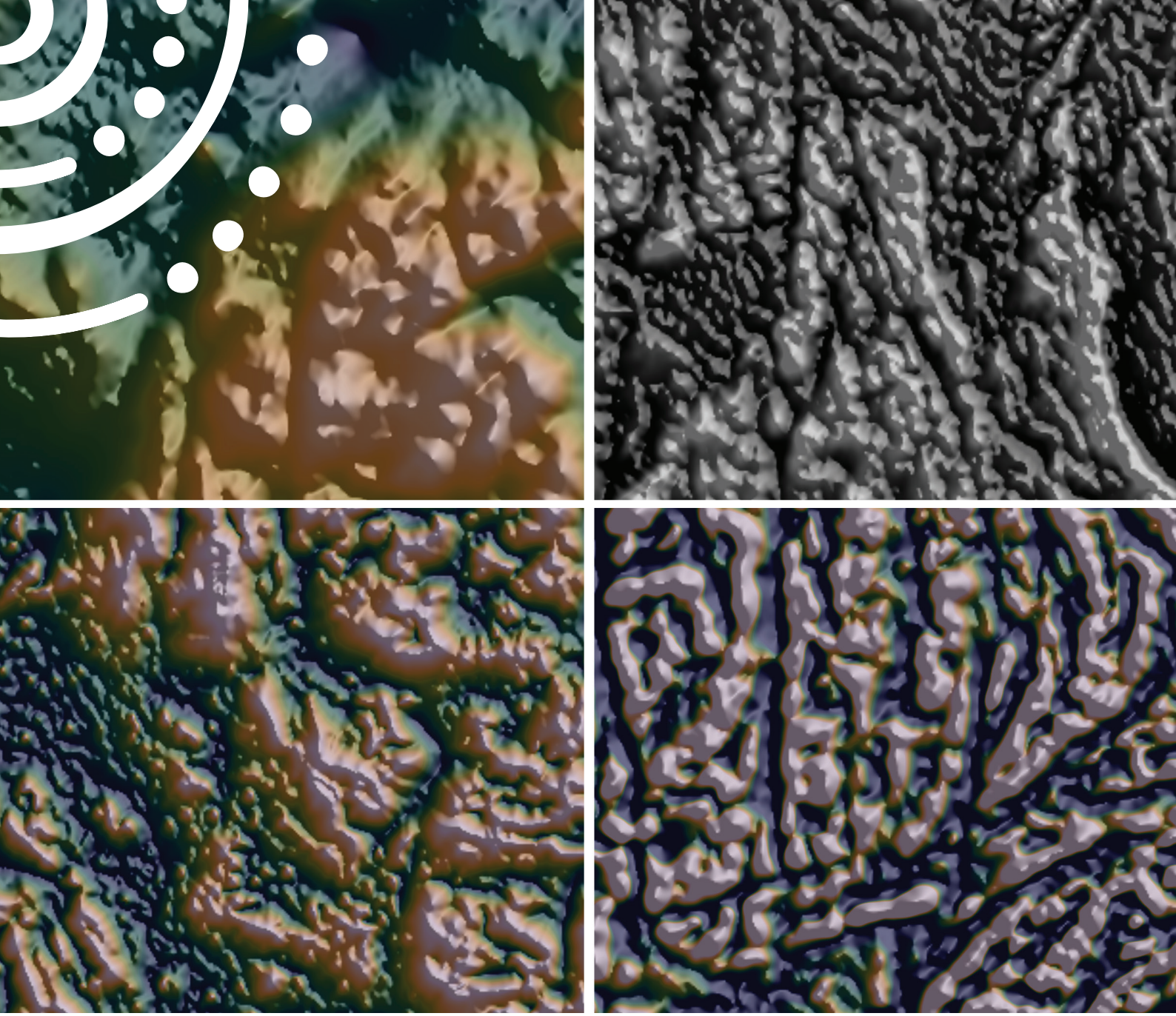

A user's guide to the Gawler Craton Airborne Survey magnetic field datasets: visualisation and interpretation

Michael McMaster, Mark Pawley, Laszlo Katona, Jonathan Irvine, Timothy Jones, George Gouthas and Tim Keeping

SOUTH AUSTRALIA

Government of South Australia
Department for Energy and Mining

A user's guide to the Gawler Craton Airborne Survey magnetic field datasets: visualisation and interpretation

Michael McMaster, Mark Pawley, Laszlo Katona, Jonathan Irvine, Timothy Jones, George Gouthas and Tim Keeping

Geological Survey of South Australia, Department for Energy and Mining

March 2023

Report Book 2023/00030

Department for Energy and Mining
Level 4, 11 Waymouth Street, Adelaide
GPO Box 320, Adelaide SA 5001
Phone +61 8 8463 3000
Email dem.minerals@sa.gov.au
dem.petroleum@sa.gov.au
www.energymining.sa.gov.au

South Australian Resources Information Gateway (SARIG)
SARIG provides up-to-date views of mineral, petroleum and geothermal tenements and other geoscientific data. You can search, view and download information relating to minerals and mining in South Australia including tenement details, mines and mineral deposits, geological and geophysical data, publications and reports (including company reports).
map.sarig.sa.gov.au

Disclaimer
The contents of this report are for general information only and are not intended as professional advice, and the Department for Energy and Mining (and the Government of South Australia) make no representation, express or implied, as to the accuracy, reliability or completeness of the information contained in this report or as to the suitability of the information for any particular purpose. Use of or reliance upon the information contained in this report is at the sole risk of the user in all things and the Department for Energy and Mining (and the Government of South Australia) disclaim any responsibility for that use or reliance and any liability to the user.

Acknowledgement of Country
The Department for Energy and Mining acknowledges Aboriginal people as the First Nations Peoples of South Australia. We recognise and respect the cultural connections as the traditional owners and occupants of the land and waters of South Australia, and that they continue to make a unique and irreplaceable contribution to the state.

Preferred way to cite this publication
McMaster M, Pawley M, Katona L, Irvine J, Jones T, Gouthas G and Keeping T 2023. *A user's guide to the Gawler Craton Airborne Survey magnetic field datasets: visualisation and interpretation*, Report Book 2023/0030. Department for Energy and Mining, South Australia, Adelaide.

CONTENTS

TABLES

FIGURES

A user's guide to the Gawler Craton Airborne Survey magnetic field datasets: visualisation and interpretation

Michael McMaster, Mark Pawley, Laszlo Katona, Jonathan Irvine, Timothy Jones, George Gouthas and Tim Keeping

INTRODUCTION

The Gawler Craton Airborne Survey (GCAS) was an airborne magnetic, radiometric and elevation survey completed in July 2019 (Katona et al. 2021a). The GCAS covers over 293,000 square kilometres (30%) of South Australia and some 55% of the Gawler Craton. The survey provides a level of detail that is significantly better than previous regional airborne surveys and thus represents a valuable resource for geoscientists (Katona et al. 2019). This is particularly the case for those areas of the Western Gawler with extensive but relatively thin (0-70m) Cenozoic cover.

Processing of the GCAS data generated a range of enhanced and derivative products; the SA Discovery Mapping project (SADM) is examining the magnetic field datasets in detail. These datasets are critical for the solid geology interpretation of the Gawler Craton, particularly for interpreting areas with only sparse basement outcrop. This report book provides a summary of the geological benefits of different magnetic field data enhancements.

The technical aspects of the different GCAS magnetic field data enhancements are well-documented well in previous publications (e.g., Foss et al. 2019, Foss et al. 2020, Katona et al. 2021a, b). The GCAS data enhancements include several commonly used derivatives, such as the reduced-to-pole TMI and the first vertical derivative of the TMI as well as less commonly used data enhancements. The latter were possible due to the internal consistency and close line spacing of the survey as well as the contiguous nature of the GCAS survey regions.

It is widely recognised that appropriate data visualisation is critical for the accurate representation and interpretation of datasets. Modern GIS software allows geoscientists to customise the visualisation of their raster datasets, for example, by using alternative colour maps or by applying hill-shading to raster data. Unfortunately, incorrect visualisation can lead to data misrepresentation, particularly if inappropriate colour maps are used. The scientific community has been discussing this issue for some time (e.g., Brewer 1994, Monmoneir 2018).

However, only recently have attempts been made to produce scientifically derived colour maps that do not visually distort data (Thyng et al. 2016, Crameri et al. 2020). Crameri et al. (2020) highlighted the need for colour maps to be true representations of the data, whilst ensuring where possible, that images are readable by users with common colour-vision deficiencies.

This report has two principal aims; the first is to highlight the geological utility and potential drawbacks of different GCAS magnetic field transformations and enhancements so that geoscientists can get the most out of these datasets. The second aim is to provide advice on how to visualise and display magnetic field datasets to help achieve the 'most accurate' geological interpretation. Please note that the examples provided in this report are based on visualisation in the ArcGIS environment, but the same principals apply, and similar techniques can be employed with other mapping software packages such as the open-source program QGIS.

THE GAWLER CRATON AIRBORNE SURVEY (GCAS)

The Gawler Craton Airborne Survey (GCAS) was an airborne magnetic, radiometric and elevation survey flown between February 2017 and July 2019. The GCAS project was undertaken by the Geological Survey of South Australia (GSSA) in collaboration with Geoscience Australia (GA) and the Commonwealth Scientific and Industrial Research Organisation (CSIRO) with the final data release occurring in February 2021 (Katona et al. 2021a, b).

The survey has 200m line spacing, ground clearance of 60m and tie-lines were flown at 2000m spacing perpendicular to the survey lines. The GCAS area is subdivided into sixteen regions or survey blocks which together cover some 530,268 square kilometres or approximately 30% of South Australia (Fig. 1). TMI data for the sixteen regions were merged into a single grid covering the entire GCAS area.

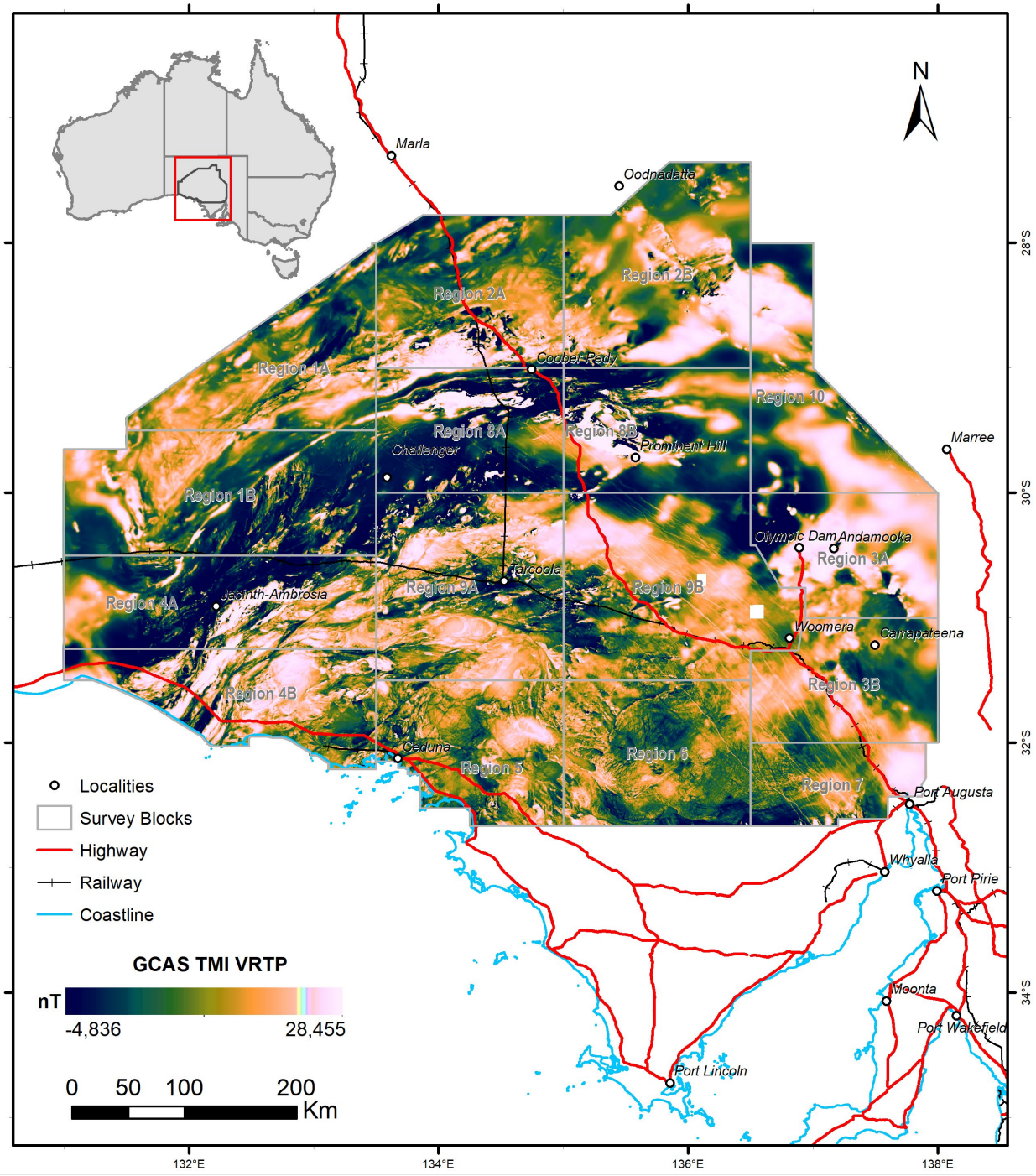

Figure 1. Location map of the Gawler Craton Airborne Survey overlain on the hill-shaded variable reduced-to-pole Total Magnetic Intensity (TMI VRTP) merged grid.

MAGNETIC FIELD DATASETS

Modern aeromagnetic surveys measure the strength in nanoteslas (nT) of the geomagnetic field, known as Total Magnetic Intensity (TMI). Local magnetic field variations are related to variations in magnetic susceptibility (***k***) which can be broadly correlated with varying proportions of ferromagnetic minerals within the rocks of an area. The variable proportion and distribution of ferromagnetic minerals can be related to the primary or secondary geological processes (Isles and Rankin 2013, Grant 1985a, b). Whereby, primary processes are related to the formation of igneous and sedimentary rocks, and they control the primary concentration (and distribution) of ferromagnetic minerals. Secondary process such as metamorphism and hydrothermal alteration can overprint primary magnetic susceptibility. These processes can lead to either an increase or decrease in ferromagnetic mineral content (principally magnetite) as well as changes in the distribution of those minerals and thus impact on the ***k*** of the body of rock (Isles and Rankin 2013). For example, fluid flow within faults and shears can lead to the destruction of magnetite (decrease in ***k*** and lower TMI) whilst metamorphic reactions can lead to the formation of secondary magnetite with an accompanying increase in ***k*** and a higher TMI response.

Different data enhancements can be applied to the TMI data to improve its utility for mapping geological features. For example, the first vertical derivative (TMI VRTP 1VD) is useful for mapping linear features and geological structures. Table 1 provides a summary of the principal data enhancements derived from the GCAS TMI dataset and how they can be used for geological interpretation. The following sections of this report provide further details on how the derivative/filters are derived from the GCAS TMI and their benefits (and drawbacks) for geological interpretation.

Table 1. GCAS magnetic field enhancements* and their importance for geological interpretation

GCAS magnetic field enhancements	Units	Utility for geological interpretation
Total Magnetic Intensity with Variable Reduction-to-Pole (TMI VRTP)	nT	Lithological mapping and mapping of alteration.
Total Gradient of TMI (TMI AS)	nT/m	Mapping of shallow intrusions including dykes.
First vertical derivative of TMI VRTP (TMI VRTP 1VD)	nT/m	Mapping of geological structures and linear features (e.g., dykes).
Second vertical derivative of TMI VRTP (TMI VRTP 2VD)	nT/m^2	Mapping of geological structures and near-surface features.
Tilt of VRTP TMI (TMI VRTP TILT)	deg. (-90 to +90°)	Mapping intrusive bodies and thin laterally continuous magnetic features (e.g., marker beds and shear fabrics).
Vertical gradient of the vertical component of TMI (TMI Bzz)	nT/m	Mapping intrusive bodies and geological features.
Pseudo gravity of TMI	$\mu m/sec^2$	Mapping of geological structures, intrusive bodies, and changes in cover thickness.
Automatic Gain Control of TMI VRTP (TMI VRTP AGC)	nT	Mapping of geological structures.
Trend and Trend Confidence of VRTP TMI 1VD	deg. (0–180°) & confidence (0–1)	Lithological mapping and mapping of dykes.

*This is not an exhaustive list of all GCAS magnetic field enhancements, rather the list contains only the derivatives/filters that are considered most useful for geological interpretation.

TOTAL MAGNETIC INTENSITY WITH VARIABLE REDUCTION-TO-POLE (TMI VRTP)

The primary dataset of the GCAS project is the Total Magnetic Intensity (TMI) with local variations in the TMI related to variations in magnetic susceptibility. TMI data can be used to map lithological contacts where there are corresponding lateral changes in magnetic susceptibility. For example, there is often a lateral variation in magnetic susceptibility across intrusive contacts and thus TMI data is useful for delineating intrusive igneous bodies.

The TMI responses of magnetic sources can be complex due to the dipolar nature of (induced) magnetism which is related to variations in the intensity and direction (inclination) of the Earth's magnetic field (Dentith and Mudge 2014). That is, the Earth's magnetic field is vertical at the magnetic poles, horizontal at the magnetic equator and inclined at mid-latitudes. The practical implication of this for the geological interpretation of magnetic data is that the TMI anomalies are not centred over their causative bodies. The GCAS area lies in the southern hemisphere and therefore the Earth's magnetic field is directed upwards and to the north resulting in asymmetrical TMI anomalies ('dipoles') with positive responses to the north of the causative bodies (Dentith and Mudge 2014, Figure 2a).

The issue discussed above can be addressed by applying the reduction-to-pole (RTP) transform to the TMI data. The RTP transform simplifies the magnetic response of a source body induced by an inclined magnetic field to the equivalent polar response where the Earth's magnetic field is vertical (Dentith and Mudge 2014). This transform centres the magnetic response over the causative bodies and thus, when interpreting magnetic data, it is preferable that reduced-to-pole (or filtered RTP equivalent) data is used to guarantee that there is minimal offset of the interpreted geological features from their actual location.

The reduction-to-pole (RTP) transform uses the International Geomagnetic Reference Field (IGRF) definition of the geomagnetic field across the area at the time of the survey, i.e., total field intensity (F- nT), inclination (I – deg.) and declination (D – deg) etc. Traditional RTP transformation uses the IGRF at the centre of the survey region to calculate the TMI RPT. The ideal RTP signal is at a maximum over a magnetic source and is only positive (Foss et al. 2020).

Unfortunately for large areas the traditional RTP correction is not ideal as there may be a significant difference between the IGRF at the centre and margins of a survey area, principally in inclination and declination but also in intensity. For reference, the inclination of the Earth's magnetic field inclination varies across South Australia from -57.5° in the north to -69.4° in the south of the state (GA 2023, NOAA 2023). A variable reduction-to-pole (VRTP) transform was applied to the merged GCAS TMI grid which improves the spatial precision of the RTP process by using multiple (variable) IGRF reference points instead of a single reference point (Katona et al. 2021b).

As discussed above TMI anomalies are often offset from the magnetic source bodies and they also tend to be broader than the corresponding anomalies in reduced-to-pole data (Figure 2). Figure 2 provides a comparison between TMI and TMI VRTP images across a portion of GCAS Survey region 4A (Barton). Note that in the TMI image the positive responses generated by the prominent magnetic features 'bleed' out to the north into the surrounding magnetic lows (Figure 2a) whereas in the TMI VRTP image the anomalies are narrower and centred over the features (Figure 2b).

Reduced-to-pole TMI images are useful for mapping lithological units particularly where there is large contrast in magnetic susceptibility between adjacent units such as igneous rocks intrusive in (meta-)sediments (Fig. 2). Shear zones and fault zones often show up as linear low magnetic zones in reduced-to-pole TMI images due to structurally controlled fluid flow/alteration which results in magnetite destruction. Linear magnetic high may also occur along structures due to the syn- to post-kinematic intrusion of igneous rocks (e.g., granites or mafic dykes) or the shearing and/or transposition of magnetic units (e.g., banded iron formations). Geological structures can be recognised in the TMI VRTP but as discussed below filters such as the first vertical derivative (1VD), tilt, Bzz and others are more useful for the mapping of geological structures.

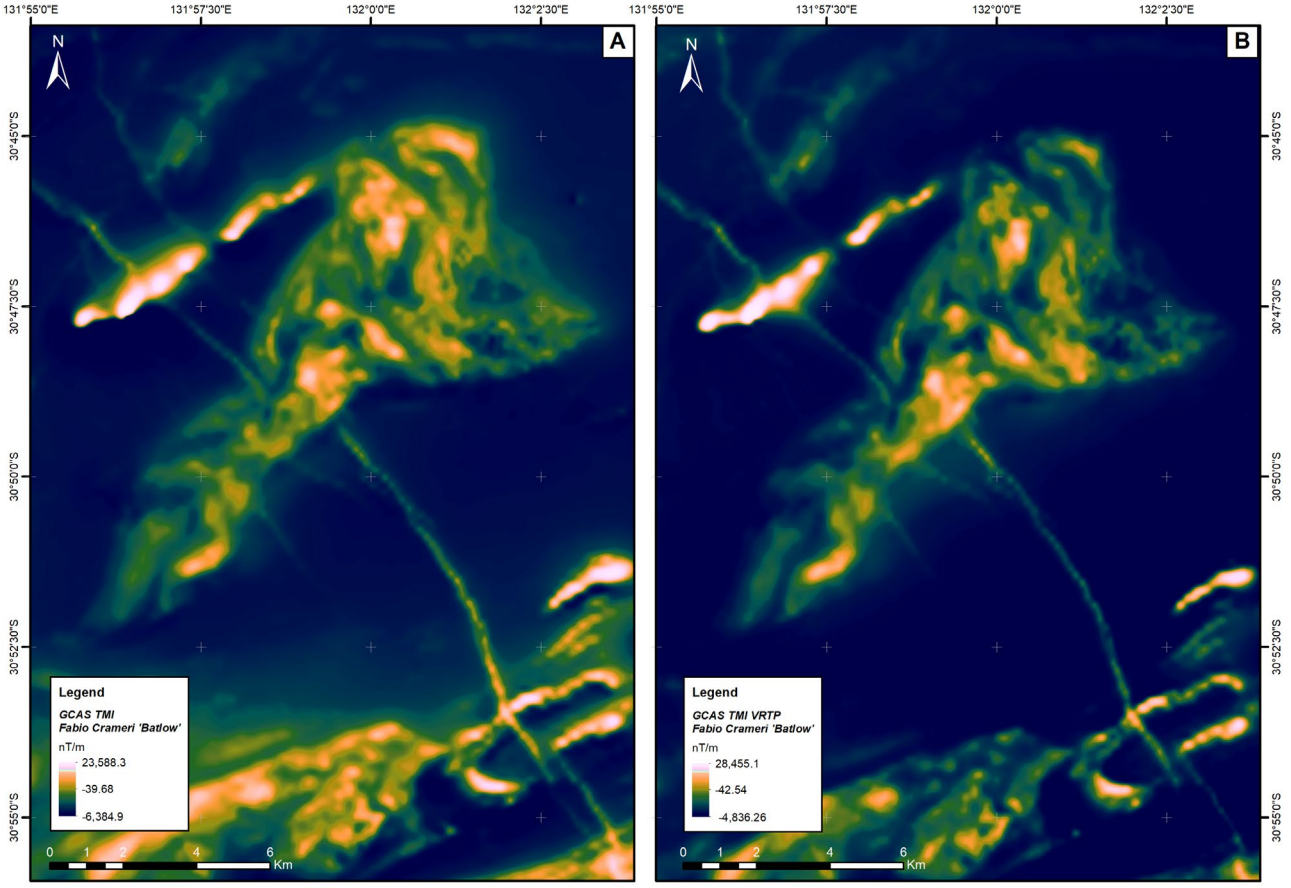

Figure 2. a) TMI and b) VRTP TMI images for part of the MOONDRAH and PIDINGA 1:100,000 map sheets (GCAS Survey Region 4A). Survey region 4A: Flown between January and May 2017, IGRF values: F - 57440 nT, I -63.4°, D +4.8° (Alken et al. 2021, Foss et al. 2019, NOAA 2023).

TOTAL GRADIENT OF TMI (TMI AS)

The 'analytical signal' of TMI (or total gradient; TMI AS) is the square root of the sum of the squares of horizontal and vertical gradients and is expressed in nT/m. The TMI AS transform has similar characteristics to the individual gradients (dX, dY, dZ), as it accentuates the response from shallow sources and improves the horizontal resolution of the magnetic field response from adjacent sources.

Therefore, this transform effectively delineates geological boundaries and maps well the distribution of shallow magnetic source bodies (Foss et al. 2020). Closely spaced, shallow intrusions such as dykes are more readily distinguished using this transform. (Foss et al. 2020). For example, the dolerite dykes of the Gairdner dyke swarm are more effectively mapped using the analytical signal of the TMI or the first vertical derivative of the VRTP TMI then with the VRTP TMI (Fig. 3).

An important advantage of the total gradient filter is that it is relatively independent of a source body's magnetisation direction (Nabigian 1984, Roest et al. 1992). As such, source bodies with strong remanent magnetism including reversely magnetised bodies can be mapped more effectively with the total gradient of TMI (Dentith and Mudge 2014, Foss et al. 2020).

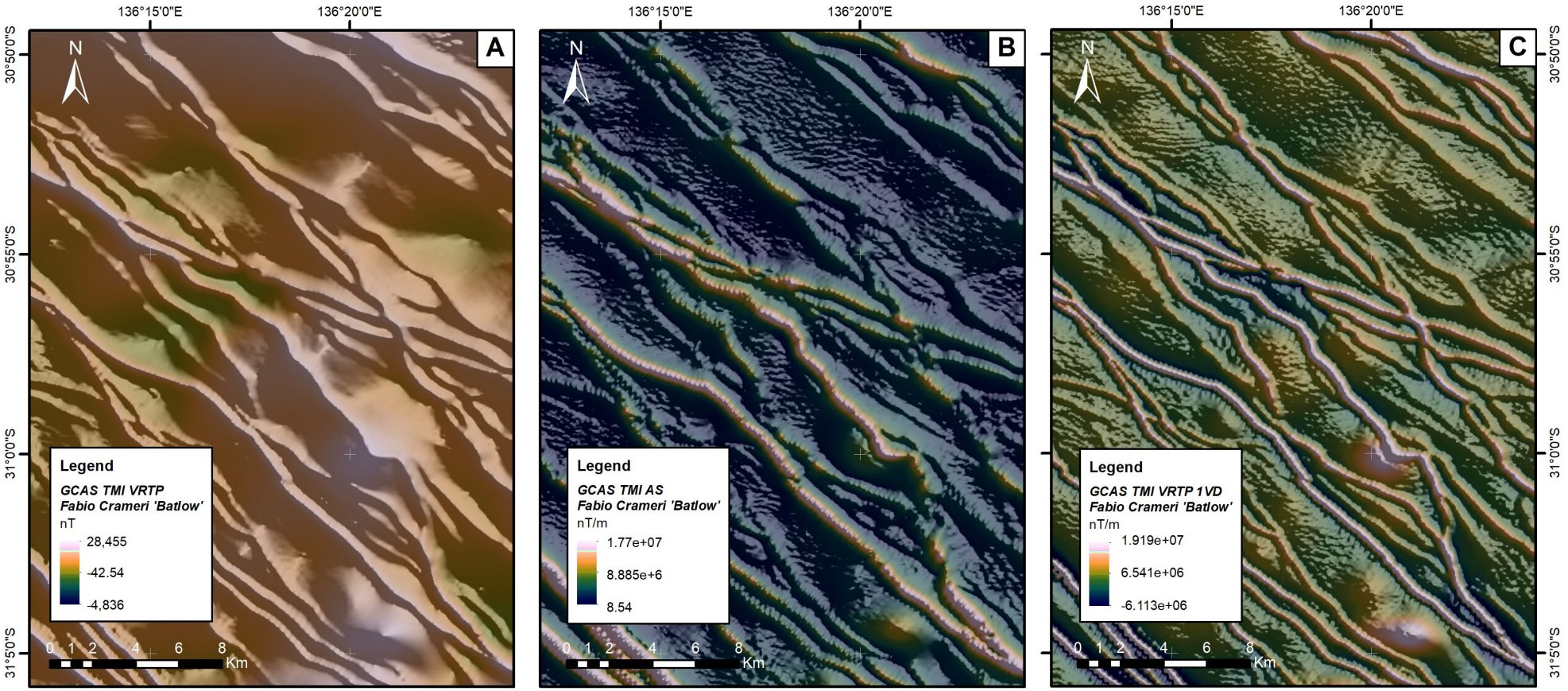

Figure 3. Comparison between a) TMI VRTP, b) TMI AS and c) TMI VRTP 1VD hill-shaded images across the Gairdner Dyke Swarm on the YOUNGHUSBAND and VIVIAN 1:100,000 map sheets.

FIRST VERTICAL DERIVATIVE OF TMI VRTP (TMI VRTP 1VD)

Gradients or derivatives of magnetic data enhance details as they are more sensitive to subsurface variations in magnetic susceptibility (Dentith and Mudge 2014). A Fast Fourier Transform (FFT) was used to calculate the first vertical derivative (or vertical gradient) of the variable reduced-to-pole TMI (TMI VRTP 1VD) which is expressed in nT/m. The vertical gradient of a field attenuates more rapidly with distance than the field itself and thus the TMI VRTP 1VD accentuates the magnetic expression of shallow sources (Fig. 3). The TMI VRTP 1VD also highlights the horizontal variation in magnetic intensity with sharper anomalies and improved lateral resolution of adjacent sources (Katona et al. 2021a).

The TMI VRTP 1VD is useful for mapping geological structures and linear features such as faults, shear zones, dykes and (magnetic) trend lines. The tilt derivative (TMI VRTP TILT) of magnetic intensity will be discussed in further detail below. However, it is worth noting that tilt produces a similar result to the first vertical derivative of TMI whilst also retaining magnetic responses from deeper sources.

SECOND VERTICAL DERIVATIVE OF TMI VRTP (TMI VRTP 2VD)

The second vertical derivative of variable reduced-to-pole TMI (TMI VRTP 2VD) is the gradient of the 1VD and is expressed in nT/m^2. The second vertical derivative filter further enhances detail in the magnetic data which visually results in sharper images than in the first vertical derivative images as shown in Figure 3c. However, the downside is that this enhancement is sensitive to short wavelength ‘noise’ in the data as well as to near- or at-surface cultural features such as railroads and buildings. The second vertical derivative also exaggerates the ‘bike-chain’ effect commonly observed in first vertical derivative images.

As per the first vertical derivative, the second vertical derivative is useful for mapping linear features such as shears, faults, and dykes. The second vertical derivative can help delineate closely spaced linear, magnetic features as the rate of change (gradient) of the first vertical derivative is greatest at their margins. Thus, two closely spaced magnetic sources will be represented as at least two distinct magnetic anomalies in the TMI VRTP 2VD image as opposed to a single, broad anomaly in the TMI VRTP 1VD image. Significantly, the second vertical derivative response is localised at the edges of magnetic sources (Denith and Mudge 2014). Therefore, the second vertical derivative is useful for mapping thin magnetic horizons (magnetic trend-lines), closely spaced dykes and (shallow) intrusive bodies. The TMI VRTP 2VD also highlights near-surface concentrations of heavy minerals related to sedimentary processes (e.g., paleochannels, strandlines or aeolian deposits).

Figure 4 compares the TMI VRTP, 1VD and 2VD images across a region of sheared paragneiss (Christie Gneiss) and orthogneiss of the Mulgathing Complex. Note the enhancement of detail in both the TMI VRTP 1VD and TMI VRTP 2VD images, with the subtle magnetic fabric of the Christie gneiss emphasised in the TMI VRTP 2VD image (Fig. 4c).

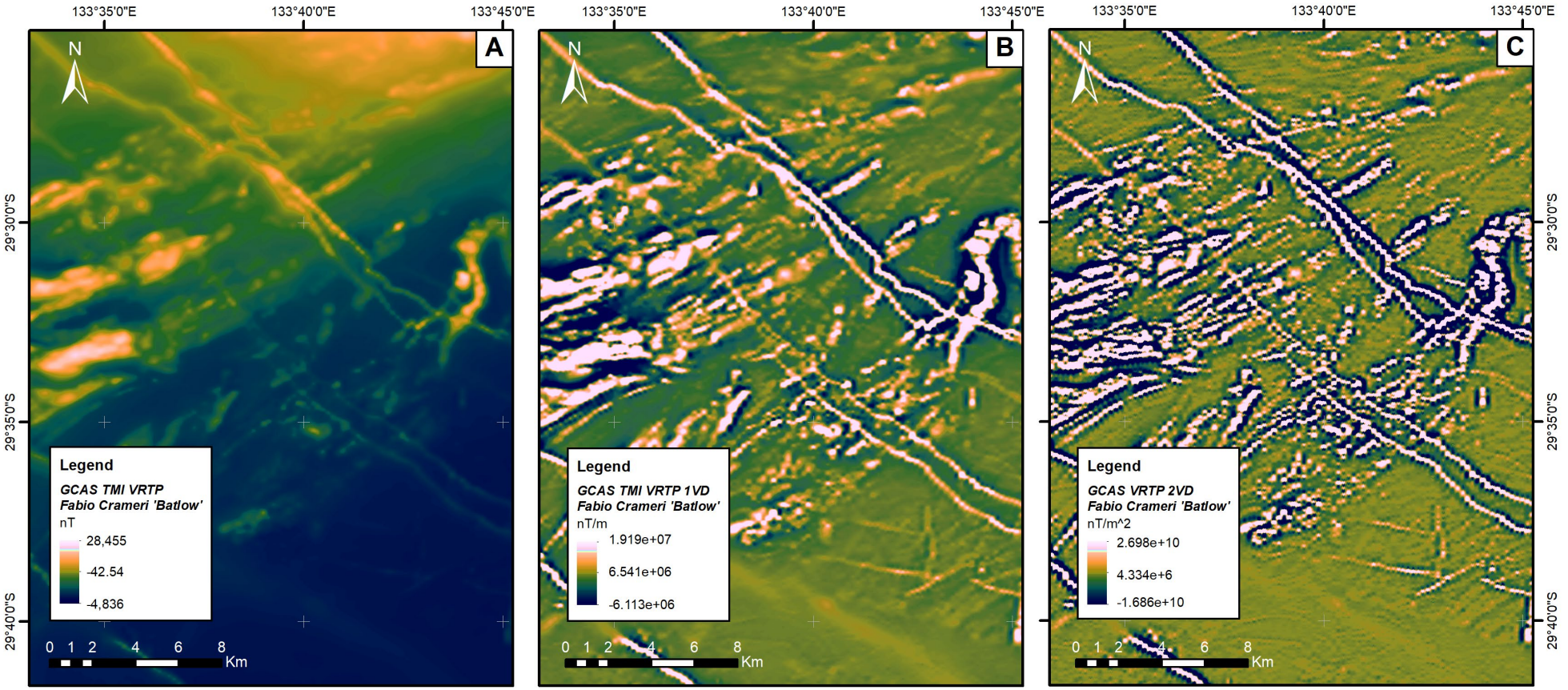

Figure 4. Comparison between a) TMI VRTP, b) TMI VRTP 1VD and c) TMI VRTP 2VD images across sheared paragneiss and orthogneiss of the Mulgathing Complex intruded by Gairdner-age dykes on the YERADA and JUMBUCK 1:100,000 map sheets.

TILT OF VRTP TMI (TMI VRTP TILT)

Tilt (or tilt angle) is the arctangent of the ratio of the first vertical derivative (1VD) and horizontal gradients of the magnetic field (Miller and Singh 1994; Verduzco et al. 2004). Due to the nature of the arctan trigonometric function, the tilt values are restricted to the range -90° to +90° (-π/2 to π/2). The ratio is independent of the amplitude of the vertical derivative or the absolute value of the total horizontal gradient (Cooper and Cowan 2006; Salem et al. 2008).

The tilt angle is positive over magnetic sources and negative elsewhere (Miller and Singh 1994). Along the edges of magnetic sources, the horizontal gradient reaches a local maximum and is significantly higher than the vertical derivative. Therefore, the zero contour (0°) of the tilt derivative approximates the outline of magnetic source bodies (Denith and Mudge 2014, Verduzco et al. 2004). In addition, the tilt derivative is useful for mapping thin, laterally continuous magnetic features such as iron-rich layers or shear fabrics (Salem et al. 2008). Thus, this dataset can be useful for understanding the magnetic fabric of an area as well as the distribution of intrusive bodies. The first vertical derivative and the tilt angle should be viewed as complementary datasets for geological interpretation. However, the TMI VRTP TILT has reduced resolution in comparison to the TMI VRTP 1VD.

The tilt derivative represents both shallow and deeper magnetic sources in a similar fashion and thus this dataset may misrepresent dipping (and folded) features. That is, the apparent location of thin magnetic layers is often offset in the TMI VRTP TILT when compared to the TMI VRTP 1VD (Fig 5). The first vertical derivative accentuates shallow features and therefore the TMI VRTP 1VD tends to highlight the shallowest portions of magnetic sources or in the case of a dipping layer the portion of that layer that is closest to the surface. In contrast, the strongest response of a magnetic feature in the tilt derivative may not represent the shallowest portion of that magnetic feature. (Verduzco et al. 2004, Salem et al. 2008).

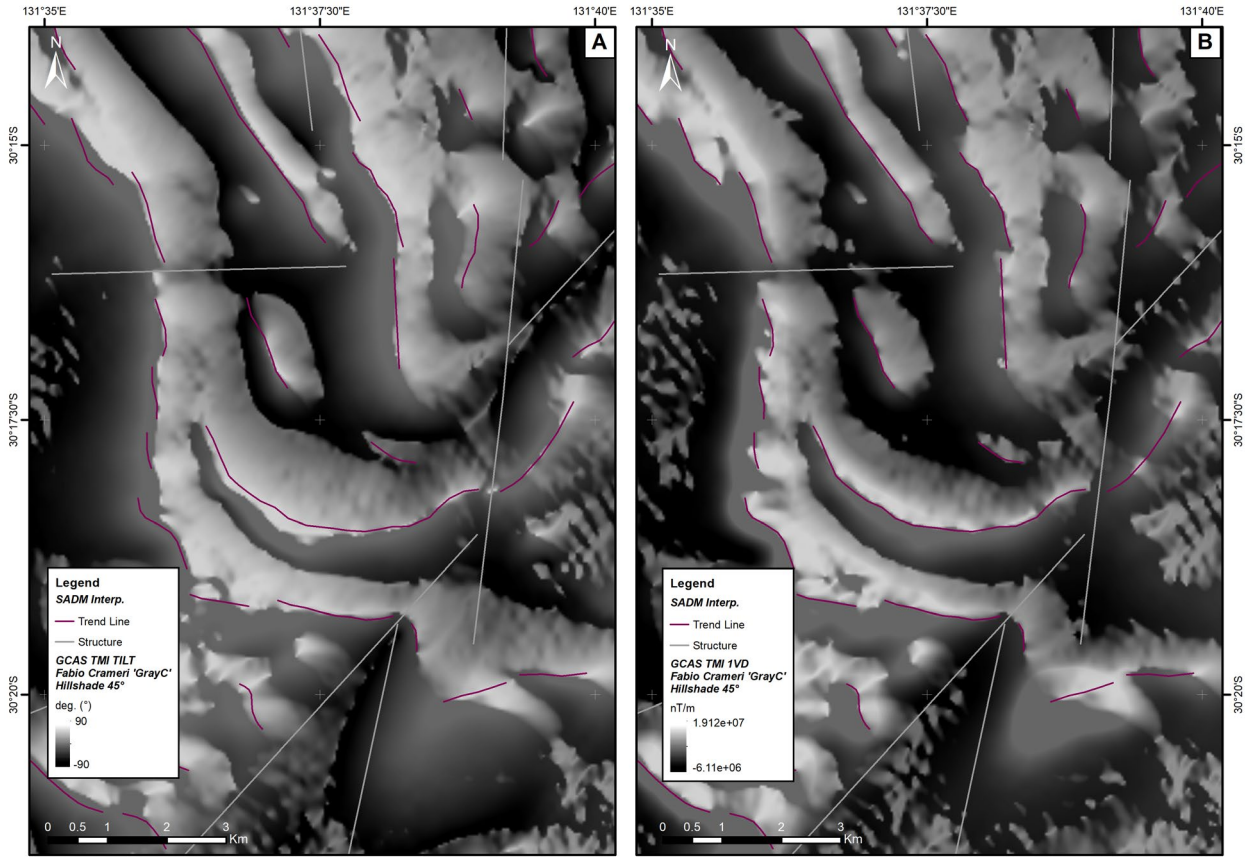

Figure 5. a) VRTP TMI TILT and b) VRTP TMI 1VD Hill-shaded images for a portion of the MARALINGA 1:100,000 map sheet with folded Fe-rich, aluminous metasediments of the Moondrah Gneiss.

This is exemplified by the contrast between the TMI VRTP TILT and TMI VRTP 1VD datasets across the folded iron-rich aluminous metasediments of the Moondrah Gneiss in the Nawa Domain of the western Gawler Craton (Fig. 5). The magnetic trend lines (purple) were mapped using the TMI VRTP 1VD and they are assumed to represent thin (folded) magnetic sources. Note that there is often an offset between these magnetic trend lines and the strongest response in the tilt derivative (Fig. 5). The positive side to the contrast between datasets is that in certain cases the direction of dip of a magnetic layer can be inferred. Nonetheless, thin, laterally continuous magnetic features/anomalies are best mapped using the first vertical derivative as the tilt can force continuity. That is, the tilt derivative can give the erroneous impression that geological features are more continuous than they are.

Bz AND Bzz (TMI Bz AND TMI Bzz)

Bzz is the vertical gradient (or first vertical derivative) of the vertical component (Bz) of the TMI. The vertical component (Bz) is derived as a phase transform of the TMI, where it is assumed that TMI is the vector in the local geomagnetic field direction (Katona et al. 2021a), i.e., the magnetic response is entirely due to induced magnetism. If this assumption is correct, then the TMI to Bz transform is independent of magnetisation direction (Lourenco and Morrison 1973). This assumption does not hold true if remanent magnetism is present. Bz provides a similar advantage to the VRTP TMI, thus it follows that the first-vertical derivative of Bz (Bzz) has similar benefits as the first vertical derivative of the VRTP TMI (Fig. 6).

Inverted colour mapping should be applied to this dataset as in the Southern Hemisphere, the Bzz filter produces a negative anomaly above a normally magnetised source (Foss et al. 2020). Bzz is expressed in nT/m and is complementary to and should be used in conjunction with the VRTP TMI 1VD, VRTP TMI TILT and VRTP TMI for mapping geological structures and the edge of magnetic bodies (Fig. 6). For the example given in Figure 6, the Bzz derivative is more effective than the VRTP TMI 1VD at delineating the intrusive contact of a deformed granite. The deformed granite of possible Kimban age (equivalent of Tunkillia Suite) is intrusive in paragneiss of the Mulgathing Complex and both basement units are cut by NW-trending, Gairdner dolerite dykes (Cowley 2008).

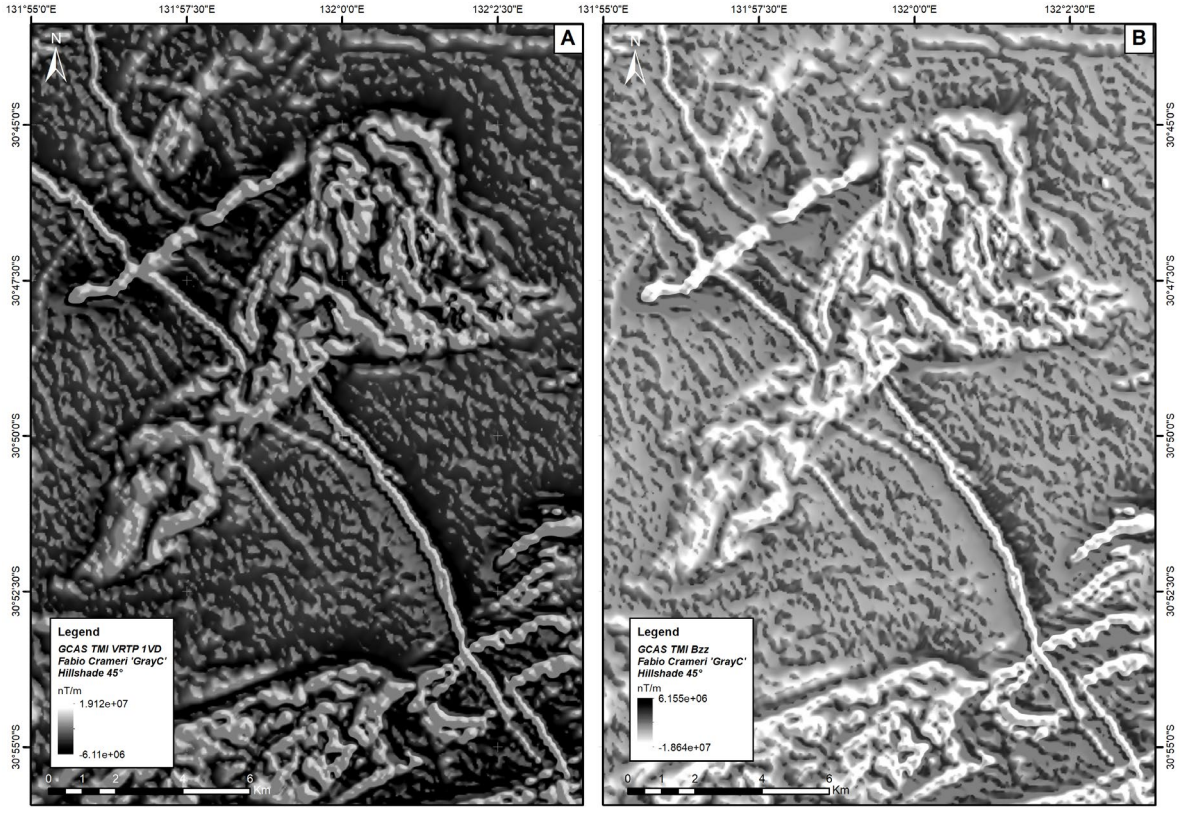

Figure 6. a) VRTP TMI 1VD and b) VRTP TMI Bzz hill-shaded images for part of the MOONDRAH and PIDINGA 1:100,000 map sheets.

PSEUDOGRAVITY

In general, detailed aeromagnetic data is more widely available and has greater coverage than detailed gravity data, and this is also the case for the majority of the GCAS area. Fortunately, the pseudogravity transform can be applied to magnetic field measurements to predict gravity field variations (Garland 1951, Baranov 1957, Bott and Ingles 1972).

The pseudogravity transform approximates gravity field data by reduction to pole and integration of the magnetic field data. The transform assumes that variations in both density and magnetic susceptibility are related to variations in ferromagnetic mineral content (e.g., magnetite) whereby density is a multiple of magnetisation with an ideal relationship of 100 kg/m^3 to 0.01 SI units. It should be noted that pseudogravity is not the actual gravity response of all the rocks in a survey area, but rather just the simulated gravity response of the magnetic rocks.

Magnetite has a specific gravity of 5.18 and consequently a buried body with elevated concentrations of this mineral would generate a magnetic anomaly and have comparable pseudogravity and Bouguer gravity anomalies. However, variations in non-magnetic mineral content can also create density contrasts, for example hematite has as specific gravity of 5.26 and as such hematite-rich rocks generate positive Bouguer gravity anomalies but don't show strong magnetic responses if they are magnetite poor. It then follows that there is only partial correlation between the pseudogravity of airborne TMI and the measured Bouguer gravity (Fig. 7 - Dentith and Mudge 2014, Foss et al. 2020). This is the case even where both datasets have comparable spatial resolution as Bouguer gravity data reflects variations in density of both magnetic and non-magnetic rocks and is also more sensitive to long-wavelength response of large and deep-seated features. Bouguer gravity and pseudogravity are both expressed in µm/sec^2.

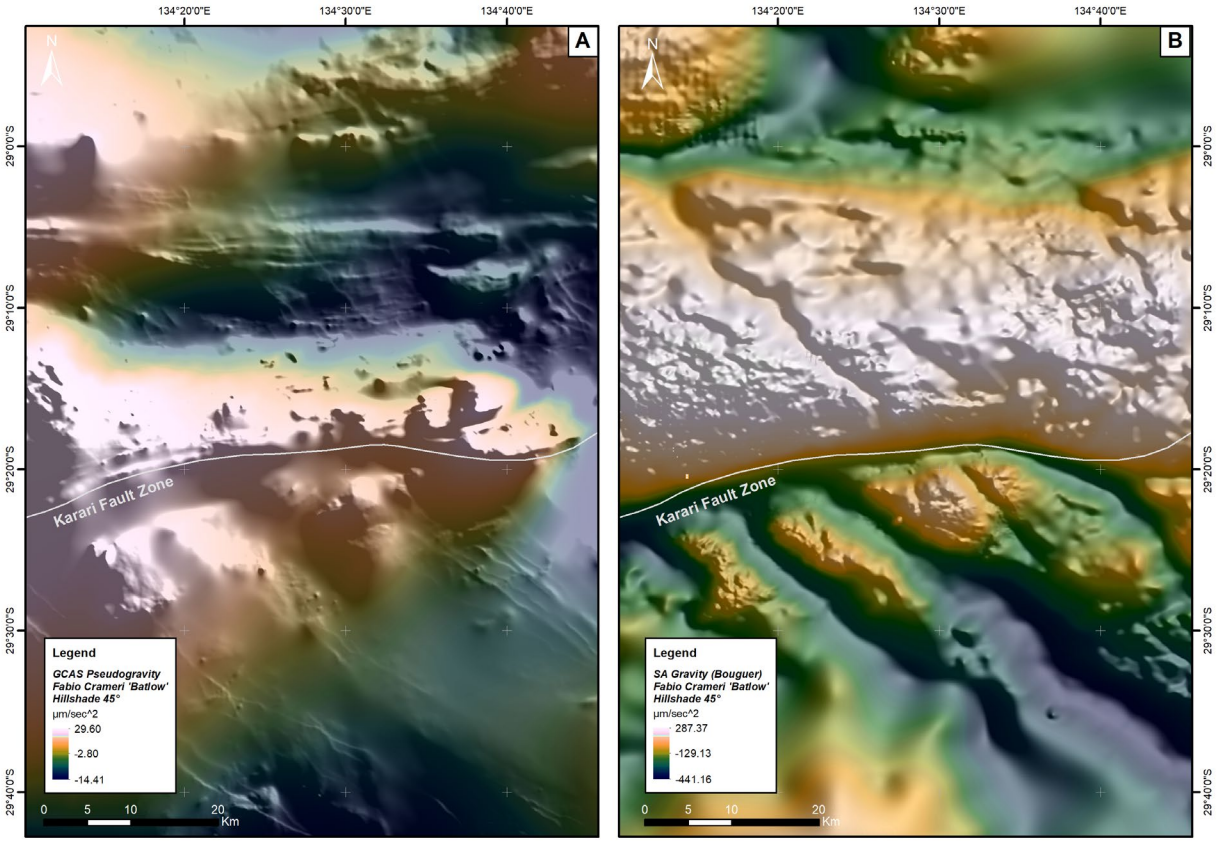

Figure 7. a) Pseudo gravity and b) Bouguer gravity hill-shaded images for part of the MABEL CREEK, ALGEBULLCULLIA, PHILLIPSON, COOBER PEDY, WOORONG and INGOMAR 1:100,000 map sheets. Dynamic range adjustment (DRA) has been applied to the colour ramps of both images.

The pseudogravity and Bouguer gravity responses across of crustal-scale structures may differ significantly due to contrasts in density driven by changes in crustal level and/or metamorphic grade, rather than variations in magnetic susceptibility. Metamorphic reactions often involve dehydration, and the resulting minerals have higher densities than those formed at lower metamorphic grades. For example, garnet forms with increasing temperature by the consumption of chlorite, which has a density of 2.6–3.3 g/m^3 whilst garnet has a density of 4.3 g/m^3. Thus, the overall density of a garnet-bearing metapelite would increase with increasing metamorphic grade (garnet growth). This change would be evident in the Bouguer gravity but not in the pseudogravity response. Figure 7 shows the pseudogravity (a) and Bouguer gravity (b) responses across the Karari Fault Zone. Note that the Bouguer gravity response is an order of magnitude greater that pseudogravity response which has a maximum value of 29.6 µm/sec^2 in contrast to a maximum Bouguer gravity response of 287.3 µm/sec^2.

The Karari Fault Zone is a major structure that separates high-grade metamorphic rocks of the Coober Pedy Ridge to the north (Daly et al. 1998; Fraser et al. 2012) from paragneisses and orthogneisses of the Archean-Paleoproterozoic Mulgathing Complex to the south (Daly and Fanning 1993; Jagodzinski et al. 2009). Iron-rich metasedimentary rocks are the dominant lithology within the Coober Pedy Ridge (Fanning et al. 2007, Jagodzinski et al. 2013), with drilling in the region intersecting quartz-magnetite-spinel-feldspar-pyroxene banded iron formations and metapelitic lithologies such as quartz–feldspar–garnet–cordierite gneiss (Fanning et al. 2007). Coober Pedy Ridge which underwent high-temperature (granulite facies) metamorphism at ca. 1600-1580 Ma (Cutts et al. 2011). The Karari Fault Zone is far more evident in the Bouguer Gravity image (Fig. 7b) largely due to the strong Bouguer gravity response of the Coober Pedy ridge to the north. Notwithstanding due the greater spatial resolution, more detail is visible in the pseudogravity image (Fig. 7a) which allows the identification of thin, NW-trending Gairdner Dolerite dykes. These dykes are strongly magnetic and thus generate strong pseudogravity responses.

The pseudogravity transform simplifies the representation of the TMI data by representing magnetic anomalies as smooth, monopole responses centred over their causative bodies. This allows easier recognition of intrusive bodies in a similar fashion to the VRTP TMI. Regional changes in depth to magnetic basement associated with changes in sediment / cover thickness are also identifiable in pseudogravity images. The pseudogravity highlights broad changes in magnetic character and can thus help delineate magnetic domains. Such magnetic domains may correspond to different crustal blocks and a comparison of pseudogravity and Bouguer gravity can help evaluate the significance of bounding geological structures. As mentioned above the Bouguer gravity response is more sensitive to deeper features and variations in crustal composition/ architecture whilst shallower features have a greater influence on the pseudogravity response.

AUTOMATIC GAIN CONTROL OF VRTP TMI (TMI VRTP AGC)

Automatic gain control (AGC) is a form of amplitude scaling that equalises the low and high amplitudes in a dataset (Rajagopalan and Milligan 1994, Denith and Mudge 2014). The resulting grid gives equal emphasis to low and high magnitude responses (Milligan and Gunn 1997). AGC images can be extremely useful for structural mapping as they can show coherent alignments not readily apparent in true amplitude data such as TMI VRTP (Rajagopalan and Milligan 1994) or TMI VRTP 1VD. This is particularly the case for ‘magnetically dull’ areas of a dataset such as portions of the western Gawler Craton that are dominated by paragneiss or in areas with thick sedimentary cover that masks the magnetic response of the underlying basement rocks.

Figure 8 shows a comparison of the TMI VRTP, 1VD and AGC images across the Karari Fault Zone. The area to the south of the fault zone is characterised by paragneiss of the Mulgathing Complex whilst to north Fe-rich, aluminous metasediments of the Nawa Domain are overlain by Neoproterozoic to Paleozoic sediments of the Officer and Arckaringa Basins. Note that subtle features and structural trends are more easily recognised in the AGC image (Fig. 8), although the AGC filter can force continuity in a similar fashion to the tilt derivative.

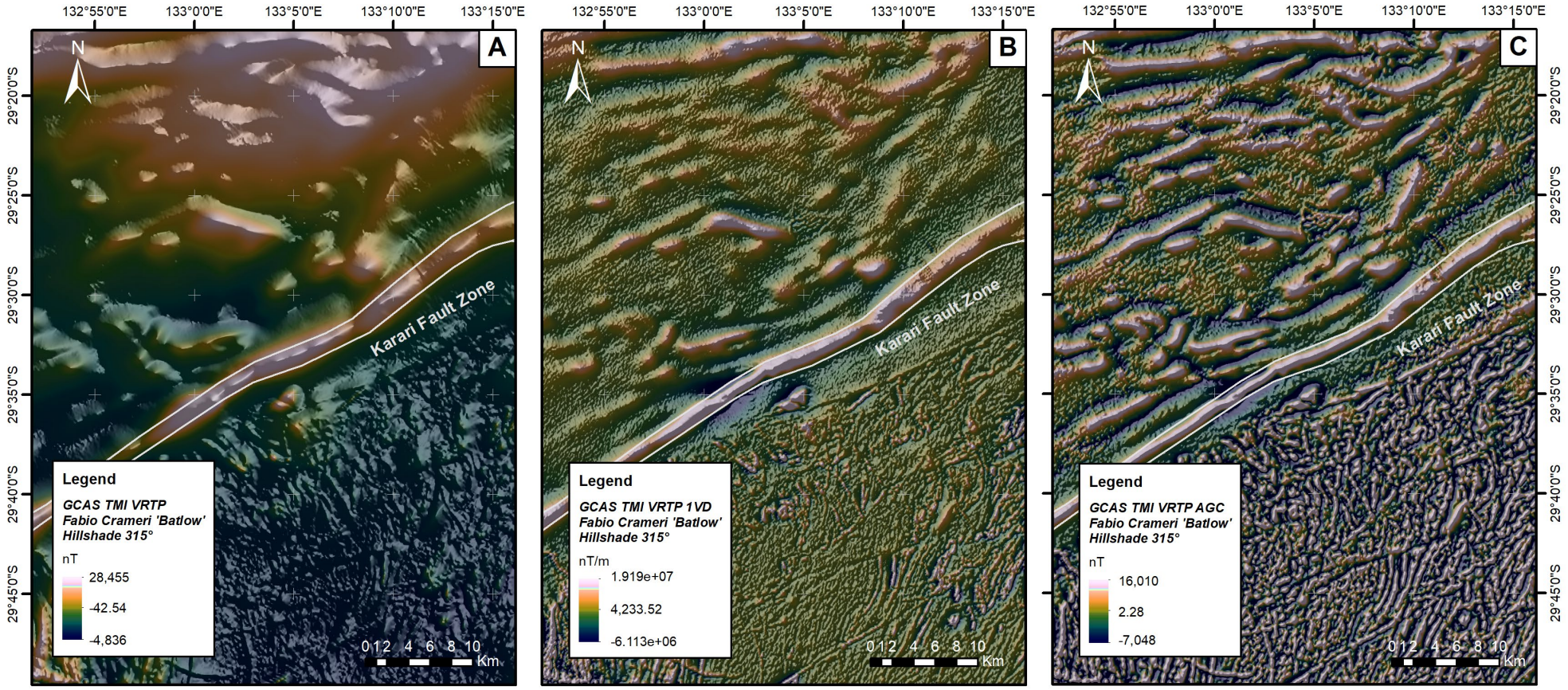

Figure 8. a) TMI VRTP, b) TMI VRTP 1VD and c) TMI VRTP AGC hill-shaded images for part of the CARNADINNA, TALLARINGA, WILKINSON, and MOONBI 1:100,000 map sheets.

TREND AND TREND CONFIDENCE OF VRTP TMI 1VD

One of the analytical products generated for each of the 16 GCAS regions were trend grids of the total magnetic intensity (TMI - Foss et al. 2019). Trend is the linear directionality of the magnetic fabric and in this case a moving window was used to calculate a spatial average. The trends grids were generated using the Grid utility tool in ModelVision and contain trend azimuth values (0-180 degree) binned within 30-degree arcs (Pratt et al. 2020, D Pratt 2023, pers. comm., 22 February).

Trend is most useful for analytics where a modeller may want to plot a profile perpendicular to a linear trend and where that trend may be difficult to interpret visually. The most common use of trend grids in ModelVision is for the automatic strike correction of AutoMag solutions which are initially calculated perpendicular to (survey) line direction (Pratt et al. 2020). AutoMag is a modelling tool which provides magnetic depth estimation in the form of modelled source bodies (Pratt et al. 2020).

Trend images by themselves are not particularly useful for the geological interpretation of the aeromagnetic data (Foss et al. 2019). However, a secondary product, trend confidence (also known as ‘trend consistency’ – Foss et al. 2019 & 2020) more clearly conveys regions of coherent trends in the magnetic data i.e., preferred orientation of magnetic anomalies (Fig. 9).

Trend confidence is calculated at the same time as trend and can be thought of a correlation coefficient that provides a confidence level (0-1) of the calculated trend value (Pratt et al. 2020). Trend confidence grids are floating point grids with values ranging from zero to one whereby the higher the value the greater the trend confidence, or confidence in the directionality of a linear feature in the grid. Values within the grids rarely exceeded 0.9. The trend confidence is computed at every non-null grid point for each bin by correlating the kernel weights of a directional cosine filter with the grid data within the angular bin / pie slice (D Pratt 2023, pers. comm., 22 February)

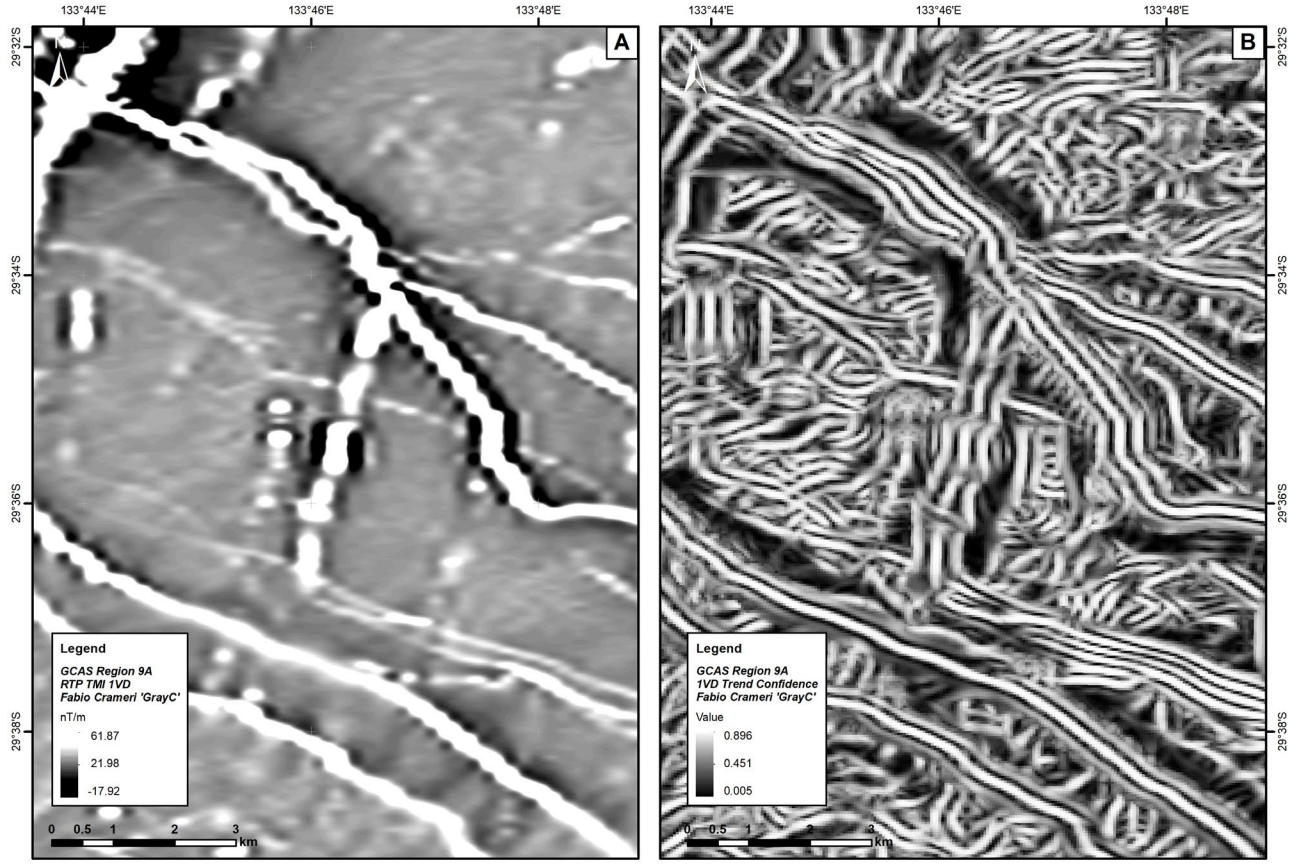

Figure 9. a) RTP TMI 1VD and b) Trend confidence images for a portion of the JUMBUCK 1:100,000 map sheet (GCAS Survey Region 8A – Coober Pedy West).

Reduced-to-pole (or filtered RTP equivalent) data should be used for geological interpretation to ensure that there is minimal offset between the magnetic response and the actual location of a geological feature. As such, trend and trend confidence grids were calculated from the first vertical derivative of variable reduced to pole TMI (VRTP TMI 1VD) grids for each of the GCAS regions (Fig. 9).

A feature of trend confidence grids is that they are not sensitive to the 'bike-chain' effect that often impacts on linear features in 1VD images (Fig. 9). Thus, trend confidence produces a more visually pleasing dataset that maps linear trends smoothly and continuously. However, the method does not distinguish between low and high values in the original data and as such every positive magnetic anomaly will have a high trend confidence anomaly on either side (Figure 9). If there is no anomaly nearby, the low trend confidence anomaly will not be as well defined as the anomaly peak (high) associated with the magnetic unit (D Pratt 2023, pers. comm., 22 February).

Contouring of the trend confidence grids was undertaken resulting in the creation of vector data (lines) that can be used for basement geology and linear feature mapping - see the case study below. "The advantage of contouring the trend confidence data is that the contours accurately capture the position of linear features in a much more time-efficient manner than by manual, on-screen digitising of the same features.

Case study: Semi-automatic dyke extraction using trend confidence

The c. 825 Ma Gairdner Dolerite dykes are laterally continuous highly magnetic features (Goode 1970; Wingate et al. 1998). Therefore, they are easily recognised as linear magnetic anomalies in the aeromagnetic data. However due to the vast number of dykes particularly in the eastern Gawler craton; the manual interpretation of dykes is a very time-consuming task particularly if mapped dykes need to be represented as polygons.

Earlier work on linking surface lineaments to basement geology in the Central Gawler craton was presented by Gonzalez-Alvarez et al. (2020) and Kelka et al. (2022). This workflow has the potential for significantly reducing the time required to undertake the geological interpretation of aeromagnetic data namely for concealed basement. The work by Gonzalez-Alvarez et al. (2020) was expanded on by Pawley et al. (2021) who developed a workflow for the automatic extraction of targeted magnetic lineaments from GCAS data, such as the Gairdner Dolerite dykes. Further work by the GSSA has established a workflow for the semi-automatic extraction of dyke contacts/boundaries which can then be used to create map polygons for individual dykes.

Due to being highly magnetic, linear, and shallow features the Gairdner dykes are readily apparent in the first vertical derivative of reduced-to-pole TMI (RTP TMI 1VD). It is therefore follows that the Gairdner dykes are also highlighted in the trend confidence grids that were generated for each the GCAS regions from the VRTP TMI 1VD images.

The trend confidence grids were contoured using contour intervals of 0.1. However, to simplify classification and display, the contour values (0.1 – 0.9) were multiplied by 10 and converted to integers and resulting 9 contour intervals were then separated into individual map layers. Of these, the '4' and '5' contours values were judged to best capture the shape, direction and lateral extent of the Gairdner Dykes and are thus considered ideal for mapping dyke boundaries. Overlaying the two preferred trend confidence contours on the trend confidence, 1VD and/or VRTP TMI images allows easy identification of the contours that correspond to the boundaries of individual dykes (Fig. 10).

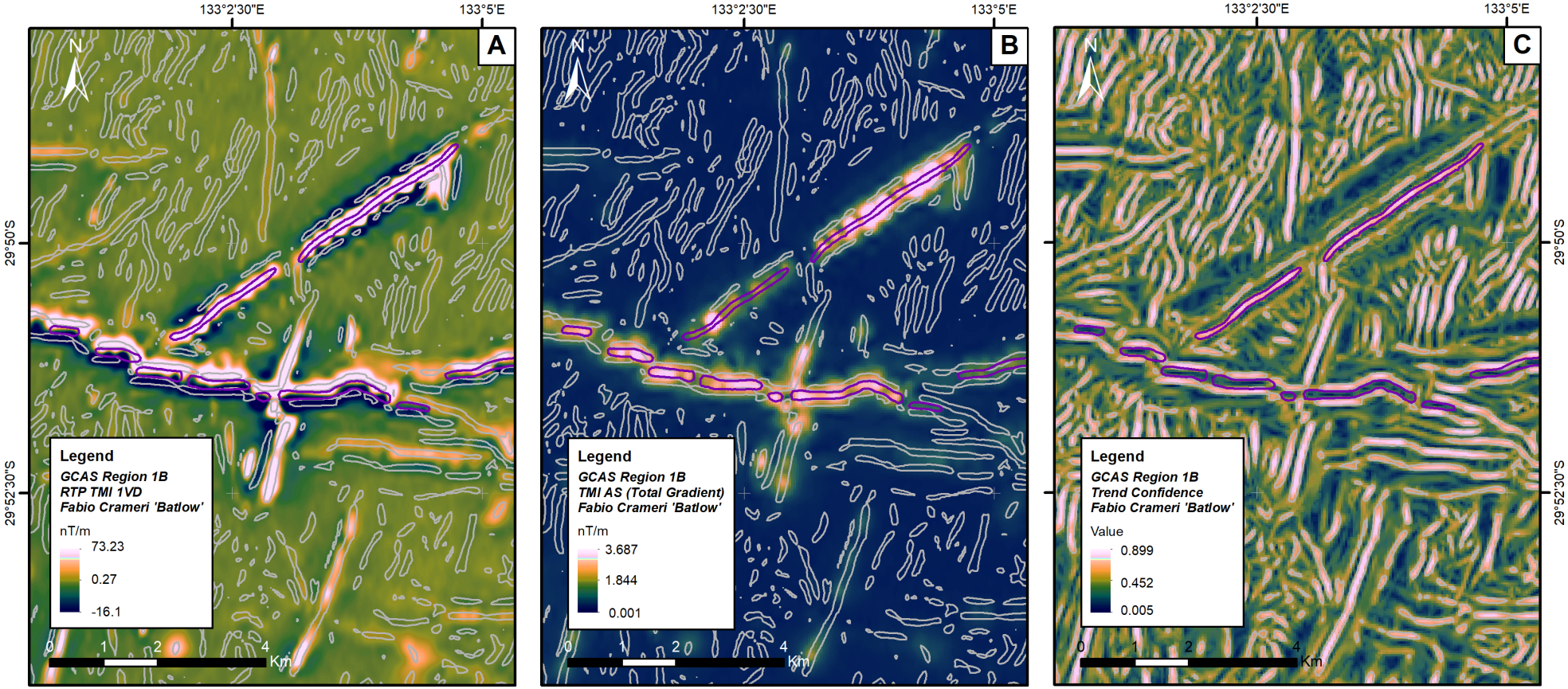

Figure 10. a) RTP TMI 1VD, b) TMI AS and c) Trend confidence images overlain by trend confidence contour '5' (grey) and interpreted dykes (purple) for a portion of the MOOONBI 1:100,000 map sheet (GCAS Survey Region 1B – Tallaringa South). Dynamic range adjustment (DRA) has been applied to the TMI AS image.

When using the trend confidence dataset interpreters should be aware of the likely direction of the features (dykes) in the area being mapped and only select the contours that best constrain their boundaries. For example, the Gairdner dolerite dykes are predominantly north-northwest (NNW) trending, however in certain regions their direction is variable such as in GCAS Region 1B (Tallaringa South; Foss et al. 2020).

Foss et al. 2002 noted that dykes in the Tallaringa South region have differing source magnetisation directions, suggesting multiple generations of dyke intrusion. Several east-west trending dykes in this region have reverse remanent magnetisation and appear as dipolar magnetic anomalies with positive and negative lobes in RTP TMI and 1VD images (Fig. 10a). Since the trend confidence images were generated from the 1VD dataset, these dykes form multiple parallel anomalies (Fig. 10c). This complexity highlights the care required when interpreting the trend confidence images (and contours) of bodies with remanent magnetism. When interpreting reversely magnetised dykes it is recommended that the trend confidence contours are overlain on the total gradient of the TMI (TMI AS – Fig. 10b) as this transform is largely independent of magnetisation direction (Nabigian 1984, Roest et al. 1992). A “GCAS Trend Confidence” data package is included as an electronic appendix and associated download to this report book.

DATA VISUALISATION

The way data is presented can have a significant impact on how the data is interpreted. This is particularly the case for raster (image) datasets such as the GCAS products. The problem of accurately representing scientific data is not a recent one but the techniques employed to visualise the data have changed significantly. Image processing techniques can be employed to better visualise raster data sets and ‘image enhancement’ is the final step in preparing aeromagnetic data for display (Jones 2022). This author presented a procedure for enhancing the GCAS magnetic datasets; namely the application of the hue, saturation, and value colour model (HSV) to the TMI VRTP grid.

However, this section of this report book will focus on key data visualisation techniques that are readily applied in mapping software packages such as ArcGIS. The authors will demonstrate how techniques such as dynamic range adjustment, shaded relief and scientific and perceptually uniform colour maps can be used to best visualise the GCAS magnetic field datasets.

As a starting point, it is worth noting that colour maps or colour ramps are fundamental to raster dataset visualisation, as they can help (or hinder) the interpretation of magnetic field datasets. For example, grayscale visualisation is recommended for several filtered datasets namely 1VD, TILT and Bzz, as the absolute amplitude of gradient values is less significant than the range of values in TMI data (Katona et al. 2021a). The development of scientific and perceptually uniform colour maps has led to the more accurate representation of raster datasets by reducing/removing the visual anomalies otherwise created by uneven colour gradients (Crameri et al. 2020). Further details on the use and benefits of perceptually uniform colour maps are provided below.

DYNAMIC RANGE ADJUSTMENT

Mapping software packages such as ArcGIS use the statistics (and histograms) of raster data to display them correctly. The statistics calculated include the minimum and maximum data values in addition to the mean and standard deviation of the raster dataset (ESRI 2019a). These statistics allow the raster data to be rendered correctly in accordance with the selected colour ramp and stretch method. For example, the VRTP TMI 1VD image shown in Figure 11A has a minimum value of -6,113,375 nT/m and a maximum value of 19,194,440 nT/m. The raster is displayed using the ‘batlow’ colour ramp and thus these maximum and minimum values are represented by white and dark blue. Note that the raster statistics were calculated for the entire dataset which in this case, represents the entire GCAS survey area.

However, it is often desirable to highlight local variations in a dataset and this can be achieved using dynamic range adjustment (DRA). Dynamic range adjustment is the process by which a

stretch is applied based only on the pixel values within the display extent and in other words the raster statistics are recalculated based on the data values within a certain (display) extent of a raster image. Figure 11B shows the same raster image (VRTP TMI 1VD) as in Figure 11A but with dynamic range adjustment applied. This highlights subtle local variations in the magnetic field data and emphasises geological structures and the metamorphic fabric of the area. Dynamic range adjustment is particularly useful in areas of low magnetic contrast such as portions of the Christie Domain or in areas of thick sedimentary cover such as the Tallaringa Trough of the Officer Basin, where a thick sequence of Neoproterozoic to Cambrian sediments masks the magnetic response of the underlying magnetite-rich, Paleoproterozoic metasediments of the Nawa Domain (Cowley 2008, Gravestock 1997).

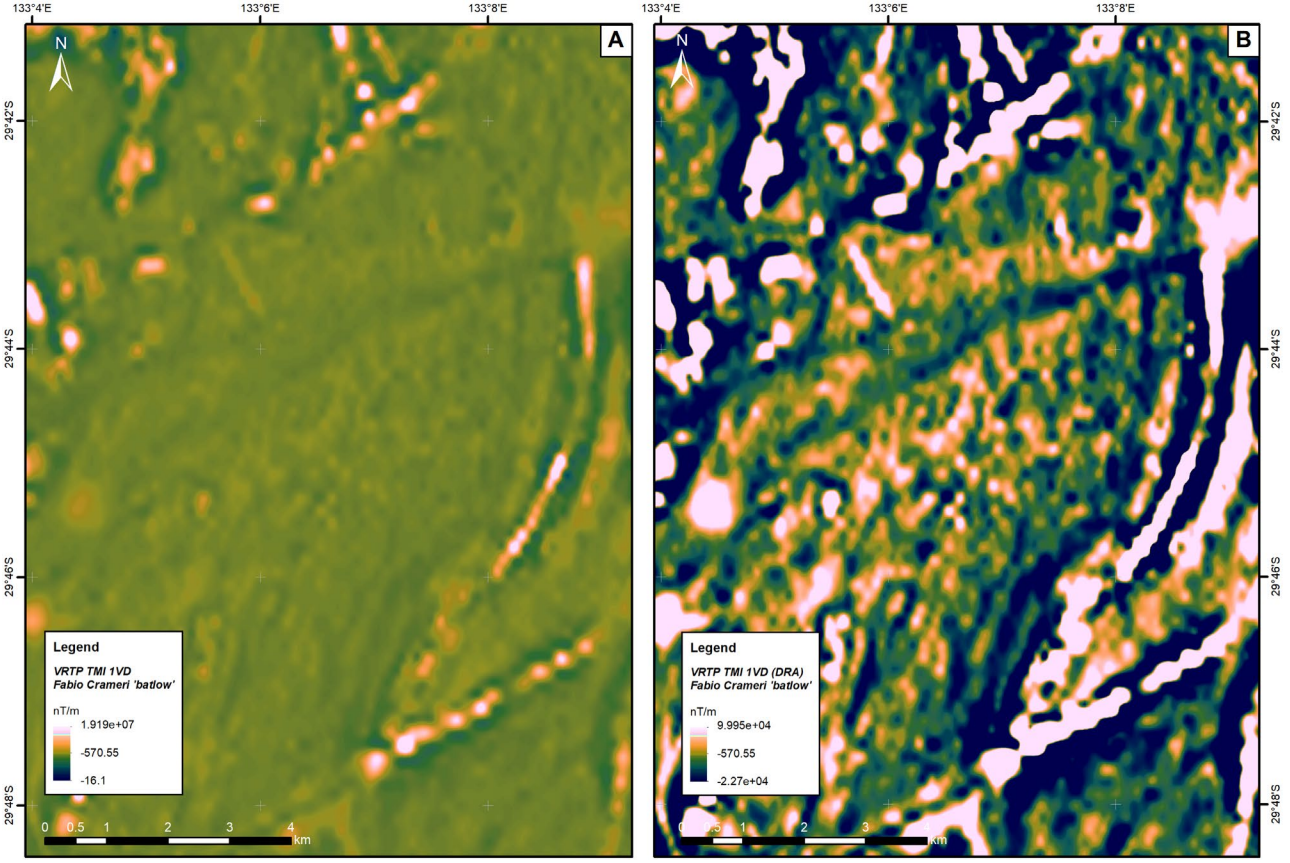

Figure 11. VRTP TMI 1VD images for part of the Moonbi 1:100,000 map sheet. a) Batlow colour ramp with default statistics/colour stretch. **b)** Batlow colour ramp with dynamic range adjustment (DRA).

SHADED RELIEF / HILL-SHADING

Many mapping software packages allow shaded relief or hill-shading to be applied to raster datasets. Shaded relief, also known as hill-shading or artificial illumination is a visual enhancement that mimics sunlight illuminating topography whereby the relief is based on the grid values, whereby higher values form 'hills' and lower values form 'valleys' (Dentith and Mudge 2014). This results in an image where the higher values cast shadows and the direction and length of the shadows are determined by the direction (azimuth) and elevation (altitude) of the illumination.

The majority of the GCAS data products can be added to an ArcGIS session as layer files with predefined hill-shading whereby the default settings are an azimuth and an altitude of 45 degrees (Katona et al. 2021). That is, the illumination is from the northeast (azimuth of 45°) at a position 45 degrees above the horizon. The Z factor or vertical exaggeration is set to 10 which increases the length of the shadows by a factor of 10.

At times it may be desirable to change these settings to emphasise features of a certain orientation. For example, illumination from the northeast (azimuth of 45°) will emphasise northwest

(NW) trending features whilst illumination from the northwest (azimuth of 315°) will highlight northeast (NE) trending features. Shaded relief images can be overlain with transparency over colour or grayscale images of the same dataset e.g., hill-shading over VRTP TMI 1VD or overlain on another dataset such as VRTP TMI.

When interpretating aeromagnetic data across areas with complex deformation histories it is beneficial to alternate between the two principal illumination directions (45° and 315°) as this will help the interpreter recognise geological structures of varying orientations. This can be achieved by overlying the hill-shading as two separate transparent overlays over the primary dataset (e.g., VRTP TMI 1VD or VRTP TMI) and turning their visibility on and off or simply viewing them together. Mapping software packages often support multi-directional hill-shading. For ArcGIS, this involves combining light from six different directions (ESRI 2019b). However, this visualisation isn't ideal for geological interpretation, rather it is better suited for the representation of topographical data.

In the context of the GCAS, the southwestern edge of the Gawler Craton is dominated by northeast and north-northeast-trending structures within the Fowler and Christie domains. Northeast (NE) and north-northeast (NNE) trending structures are more readily identified and mapped by using hill-shading with a light source from the northwest (azimuth of 315°; Fig. 12a). For example, the NNE trending, crustal-scale Tallacootra Shear Zone (TSZ) is visible in the lower left of both images, however the feature is more apparent in the hill-shaded image with illumination from the northwest (Fig. 12a). Whilst the north-northwest trending Gairdner dykes are emphasised by the shaded relief image with illumination from the northeast (Fig. 12b).

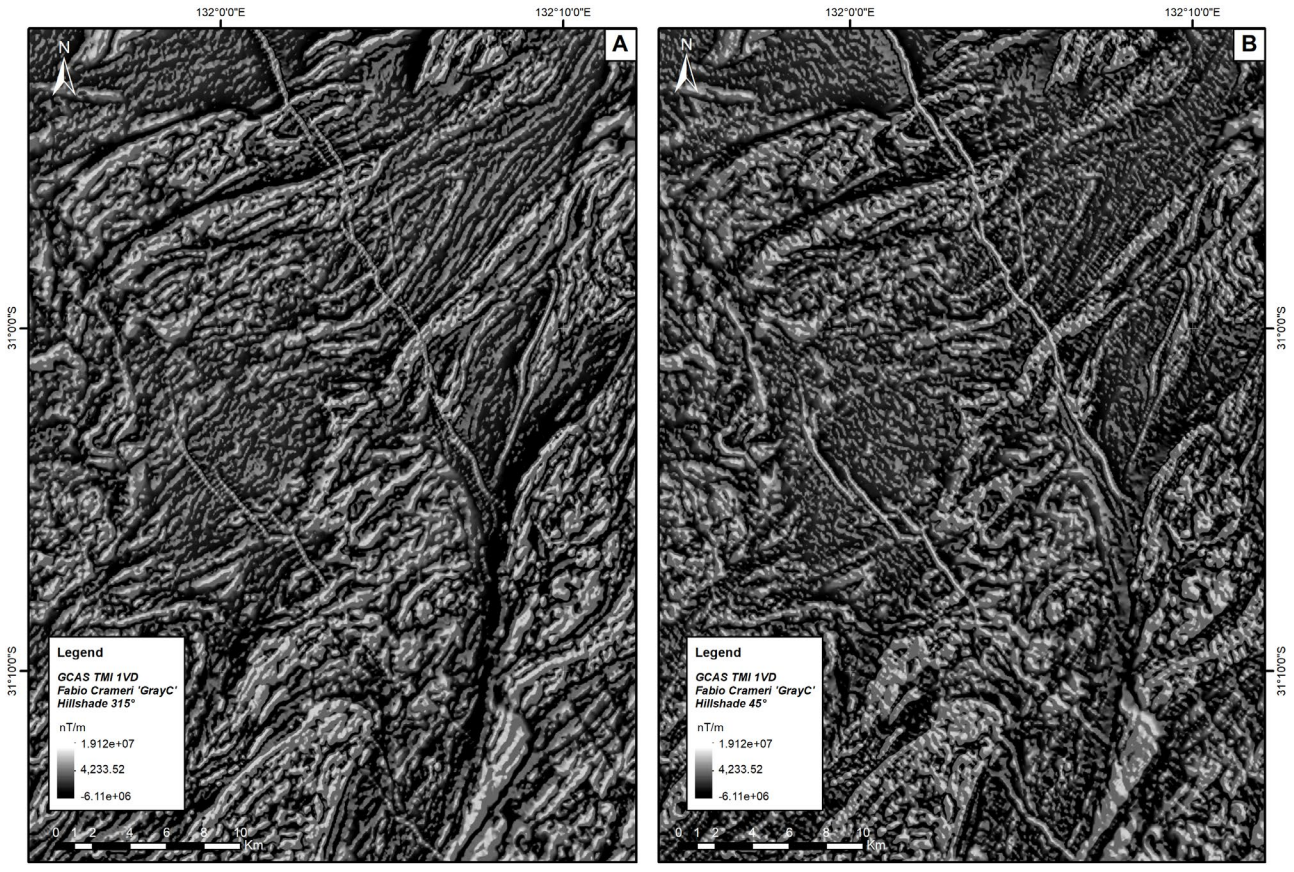

Figure 12. VRTP TMI 1VD hill-shaded images for part of the MOONDRAH, PIDINGA, YALATA and TALLACOOTRA 1:100,000 map sheets. a) Illumination from the northwest (azimuth of 315°). **b)** Illumination from the northeast (azimuth of 45°).

PERCEPTUALLY UNIFORM COLOUR MAPS

All scientists must deal with the problem of how to accurately represent scientific data. Unfortunately most commonly applied colour maps (for raster datasets) visually distort data, particularly the rainbow (jet) colour map. These colour ramps often create 'visual' anomalies which do not correspond to real data anomalies but rather are related to how the human eye perceives colour and variations in colour (Crameri et al. 2020). Traditional colour maps have the added disadvantage of not being universally accessible because their colour combinations are often not readable by those who are colour-vision deficient or colour-blind (Crameri et al. 2020). Crameri (2018a, b) developed a suite of open-access, scientific, colour-vision deficient friendly schemes and perceptually uniform colour maps (ramps) which were used to elaborate the figures presented in this report book.

Visual anomalies are related to the way the human eyesight has evolved leading to a strong bias towards the orange-red part of the visible light spectrum. As such, when viewing scientific figures that use the rainbow colour map the viewer's eyes are drawn to the yellow, orange, and red tones whilst the blue and green parts of the figure are essentially ignored (Crameri 2017). A good example of this phenomenon is seen in a global map of the ocean seafloor ages centred on the Pacific Ocean (Fig. 13a). The rainbow colour map (Geosoft Rainbow1) creates apparent 'breaks' in seafloor age, the most obvious of which are the transitions from white to red and yellow to green. In contrast when perceptually uniform colour maps, such as the 'vik' colour map, are used these apparent breaks disappear and local data variations become more apparent (Fig. 13b). The vik colour map used in Figure 13b highlights the large area of similar age (~100 Ma) oceanic crust which lies to the northeast of Fiji, Tonga, and the Tonga trench. This area of ~100 Ma oceanic crust is bounded by younger (~85–90 Ma) crust to the south. However, the rainbow colour ramp used in Figure 13a hides this and other local data variations in the greenish and cyan portions of the map. The two map insets show more detailed views of the Fiji-Tonga region.

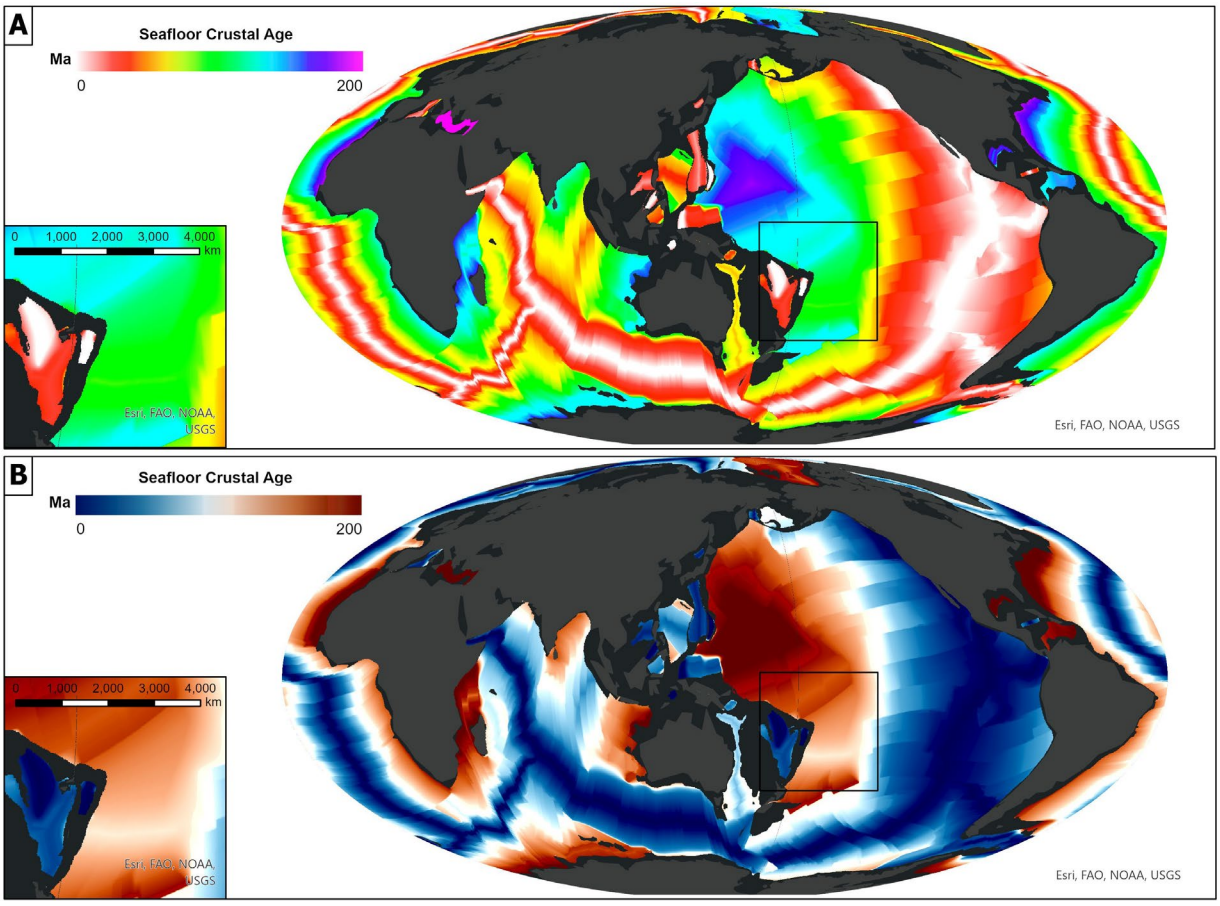

Figure 13. Global ocean seafloor ages after Muller et al. 2008. a) Rainbow colour map (Geosoft Rainbow1). **b)** Perceptually uniform colour map (Fabio Crameri vik).

In the context of the GCAS, visual anomalies are identifiable when comparing the same magnetic field datasets displayed with traditional rainbow colour maps and perceptually uniform colour maps such as the batlow colour map developed by Crameri (2018). Figure 14 demonstrates such a comparison for a TMI VRTP anomaly centred on a moderately to highly magnetic granitoid intrusion within gneisses of the Mulgathing Complex in the Christie Domain of the western Gawler Craton. When visualised with the Geosoft Rainbow1 colour scheme, the VRTP TMI dataset displays distinctive visual breaks at the transition from red/orange to yellow (c. 100 nT) and from green to cyan (c. -140 nT; Fig. 14a). This creates the impression that there are significant breaks in the data at these values and that the orange-red colours represent distinctive magnetic bodies within the larger intrusive. It should be noted that magnetic susceptibility often varies across an intrusive body due to variation in the concentration of ferromagnetic minerals, namely magnetite (Clark 1997). However, it is likely that the boundaries defined by the c. 100 nT contour in Figure 14a are not geologically meaningful, rather they are artifacts of the colour ramp used.

The main intrusive contact is emphasised by both colour ramps however in contrast to the batlow colour map, low magnetic values are represented by the colour magenta with the Geosoft Rainbow1 colour map. This creates the impression of geologically significant boundaries within the basement rocks at the transition from blue to magenta. The perceptually uniform batlow colour ramp highlights subtle variations in magnetic intensity within moderately magnetic portions of the intrusions (Fig. 14b). These variations are hidden within the green and cyan portions of the rainbow colour scheme (Fig. 14a). As discussed above; it is recommended that dynamic range adjustment and hill-shading be used to highlight local variations in magnetic intensity and geological structures, respectively.

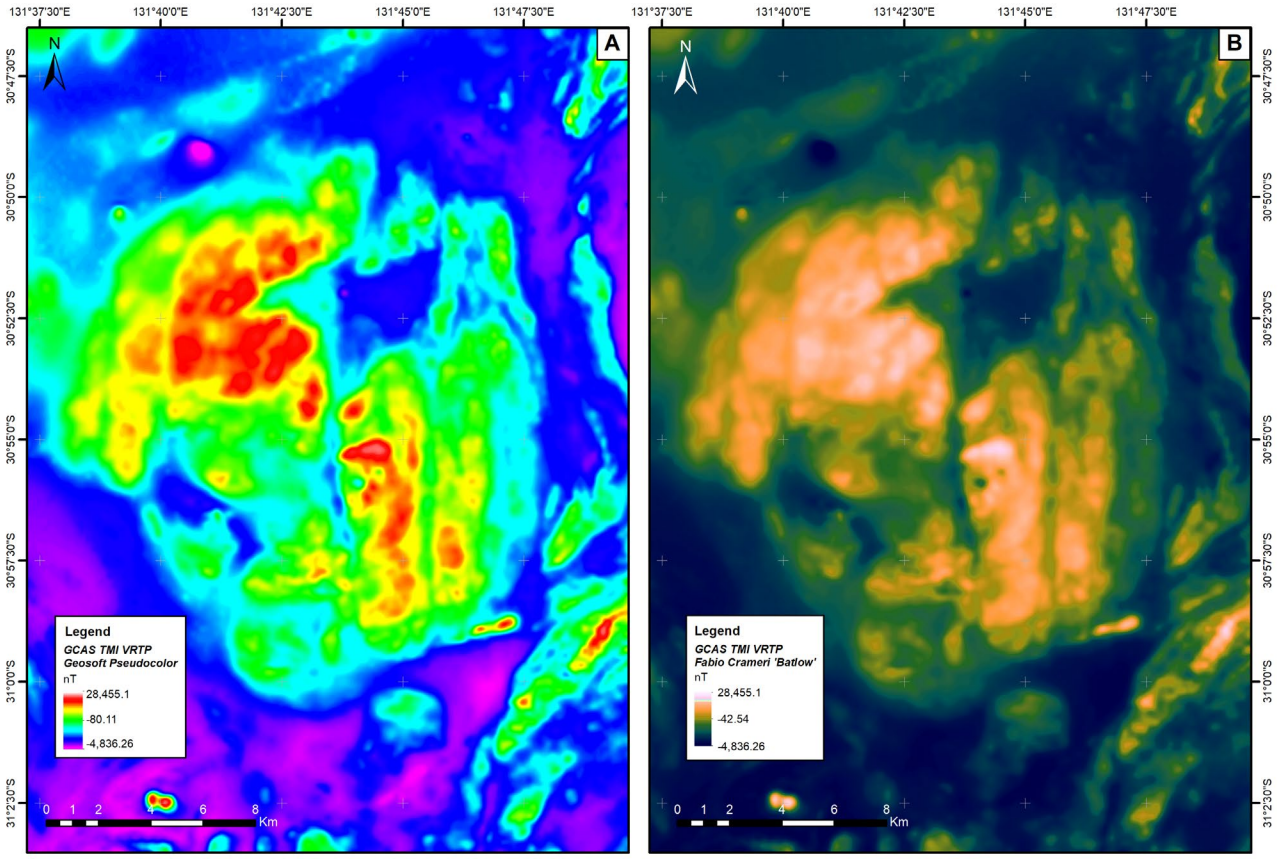

Figure 14. TMI VRTP images of a c. 15 km-wide granitoid intrusion, MOONDRAH 1:100,000 map sheet. Centre coordinate of granite body – Lat. 31°05'27"S, Long. 131°43'41"N. **a)** Traditional rainbow colour scheme (Geosoft Rainbow1). **b)** Perceptually uniform colour map (Fabio Crameri batlow).

CONCLUSIONS

The Gawler Craton Airborne Survey Project delivered a wide range of magnetic field enhancements derived from the primary magnetic dataset, the total magnetic Intensity (GCAS TMI). The different magnetic field datasets provide varying benefits for the purpose of geological interpretation and as such the data enhancements should not be viewed in isolation. Instead, multiple filters and derivatives need to be considered during the geological interpretation of magnetic data. This also holds true for the interpretation of other geophysical datasets such as gravimetric and radiometric data.

The differences between filtered datasets are often subtle but their comparison leads to the recognition and refinement of interpreted geological features which ultimately enriches the final geological map. The interpreter should have a good understanding of the physical basis of the geophysical data being interpreted and understand what is being represented, in geological terms, by the different filters and data enhancements.

A coherent geological interpretation also depends on appropriate data visualisation to avoid the misinterpretation of geological features and to minimise visual anomalies The correct data visualisation and the comparison of a variety of different field enhancements will ensure that the resulting interpretative map is as close as possible to reality. The interpreter should endeavour to ask themselves the following question: Is my interpretation (of the geophysical data) geologically credible and does it fit the data?

REFERENCES

Alken P, Thébault E, Beggan CD et al. 2021. International Geomagnetic Reference Field: the thirteenth generation. *Earth Planets Space* 73 (49). doi:10.1186/s40623-020-01288-x

Baranov V 1957. A new method for interpretation of aeromagnetic maps: pseudo-gravimetric anomalies. *Geophysics* 22:359–383. doi:10.1190/1.1438369

Bott MHP and Ingles A 1972. Matrix methods for joint interpretation of two-dimensional gravity and magnetic anomalies with application to the Iceland-Faeroe Ridge. *Geophysical Journal of the Royal Astronomical Society* 30: 55–67. doi:10.1111/j.1365-246X.1972.tb06179.x

Brewer CA 1994. Chapter 7 - Color Use Guidelines for Mapping and Visualization. In AM MacEachern and DR Fraser Taylor eds. Modern Cartography Series. *Academic Press* 2: 123–148. doi:10.1016/B978-0-08-042415-6.50014-4.

Cooper GRJ and Cowan DR 2006. Enhancing potential field data using filters based on the local phase. *Computers and Geosciences* 32: 1585–1591.

Cowley WM (Compiler) 2008. Solid Geology South Australia, Archaean to Ordovician, 1 : 2,000,000 scale. Department of Primary Industries and Resources South Australia. Available via SARIG

Clark DA 1997. Magnetic petrophysics and magnetic petrology: Aids to geological interpretation of magnetic surveys. *AGSO journal of Australian geology & geophysics* 17(2): 83-103 (Open Access).

Crameri F 2017. *The Rainbow Colour Map (repeatedly) considered harmful*. Geodynamics Division, European Geosciences Union accessed 12 April 2022.

Crameri F 2018a. *Scientific colour maps (7.0.1)*. Zenodo. doi:10.5281/zenodo.5501399, accessed 12 April 2022.

Crameri F 2018b. Geodynamic diagnostics, scientific visualisation and StagLab 3.0. *Geoscientific Model Development*, 11: 2541-2562, doi:10.5194/gmd-11-2541-2018 (Open Access)

Crameri F, Shephard GE, and Heron PJ 2020. The misuse of colour in science communication. *Nature Communications* 11: 5444. doi:10.1038/s41467-020-19160-7 (Open Access)

Cutts, K, Hand M and Kelsey DE 2011. Evidence for early Mesoproterozoic (ca. 1590 Ma) ultrahigh-temperature metamorphism in southern Australia. *Lithos* 124: 1-16. doi:10.1016/j.lithos.2010.10.014

Daly SJ and Fanning CM 1993. Archaean. In Drexel, JF, Preiss WV and Parker AJ eds, *The geology of South Australia; Volume 1, The Precambrian*. Geological Survey of South Australia. Bulletin 54, Adelaide, South Australia, Australia, pp. 32-49.

Daly SJ, Fanning CM and Fairclough MC 1998. *Tectonic evolution and exploration potential of the Gawler craton*. South Australia: *AGSO Journal of Australian Geology and Geophysics* 17: 145–168.

Denith M and Mudge ST 2014. *Geophysics for the mineral exploration geoscientist*. Cambridge University Press, Cambridge.

ESRI 2019a. *Raster data statistics - ArcMap 10.7*. ESRI [webpage], accessed 31 January 2023.

ESRI 2019b. *Hillshade function - ArcMap 10.7*. ESRI [webpage], accessed 06 January 2023.

Fanning CAM, Reid AJ and Teale G 2007. *A geochronological framework for the Gawler Craton, South Australia*. South Australia. Geological Survey. Bulletin 55.

Foss CA, Gouthas G, Katona LF, Wise TW and Pawley MJ 2019. *PACE Copper Gawler Craton Airborne Survey, Region 4A, Barton – enhanced geophysical imagery and magnetic source depth models.* Report Book 2019/00012. Department for Energy and Mining, South Australia, Adelaide.

Foss CA, Gouthas G, Wise T, Katona LF, Hutchens MF, Reed GD and Heath PJ 2020. *Gawler Craton Airborne Geophysical Survey Region 9B, Kingoonya – Enhanced geophysical imagery and magnetic source depth models*. Report Book 2020/00018. Department for Energy and Mining, South Australia, Adelaide.

Fraser G and Lyons P 2006. Timing of Mesoproterozoic tectonic activity in the northwestern Gawler Craton constrained by 40Ar/39Ar geochronology. *Precambrian Research.* 151: 160-184. doi:10.1016/j.precamres.2006.08.007

Fraser AR, Reid A and Stern RA 2012. Timing of deformation and exhumation across the Karari Shear Zone, north-western Gawler Craton, South Australia. *Australian Journal of Earth Sciences* 59: 547-570. doi:10.1080/08120099.2012.678586

Garland GD 1951. Combined analysis of gravity and magnetic anomalies. *Geophysics* 16: 51–62. doi:10.1190/1.1437650

Geoscience Australia 2023. Australian Geomagnetic Reference Field Values [data service], Geoscience Australia. accessed 28 March 2023.

Gonzalez-Alvarez I, Krapf CBE, Kelka U, Martinez C, Albrecht T, Ibrahimi T, Pawley MJ, Irvine JA, Petts, AE, Gum JC and Klump J 2020. *Linking cover and basement rocks in the Central Gawler Craton*, South Australia. Report Book 2020/00029. Department for Energy and Mining, South Australia, Adelaide.

Grant FS 1985a. Aeromagnetics, geology and ore environments, I. Magnetite in igneous, sedimentary and metamorphic rocks: an overview. *Geoexploration* 23: 303–333. doi:10.1016/0016-7142(85)90001-8

Grant FS 1985b. Aeromagnetics, geology and ore environments, II. Magnetite and ore environments. *Geoexploration* 23: 335–362. doi:10.1016/0016-7142(85)90002-X

Gravestock DI 1997. Geological Setting and Structural History. In Morton JGG and Drexel JF eds, *The petroleum geology of South Australia. Vol 3: Officer Basin*. South Australia. Department of Mines and Energy Resources. Report Book, 97/19:7-22.

Isles DJ and Rankin LR 2013. *Geological interpretation of aeromagnetic data*, Australian Society of Exploration Geophysicists (ASEG), Perth

Jagodzinski EA, Reid AJ and Dutch R 2013. *Zircon and monazite geochronology via SHRIMP and LA-ICPMS for the northern Gawler Craton, from 2009 GOMA Drilling*, Report Book 2013/00013. Department for Manufacturing, Innovation, Trade, Resources and Energy, South Australia. Adelaide.

Jagodzinski E, Reid A and Fraser G 2009. *Compilation of Shrimp U-Pb geochronological data for the Mulgathing Complex, Gawler Craton, South Australia, 2007-2009*. Report Book 2009/16, Department of Primary Industries and Resources, South Australia, Adelaide.

Jones T 2022. Aeromagnetic images of the Gawler Craton: enhancements serving geological interpretation using the HSV colour model. *MESA Journal* 097: 004-009. Department for Energy and Mining, South Australia, Adelaide.

Katona L, Hutchens M and Foss C 2019. Geological Survey of South Australia: An overview of the Gawler Craton Airborne Survey – new data and products. *Preview* 200: 24-26. https://doi.org/10.1080/14432471.2019.1625502 (Open access)

Katona LF, Reed GD and Heath PJ 2021a. *Gawler Craton Airborne Survey 2017–2021: final report.* Report Book 2021/00017. Department for Energy and Mining, South Australia, Adelaide.

Katona LF, Reed GD, Heath PJ, Gouthas G and Irvine JA 2021b. *The Gawler Craton Airborne Survey. Total Magnetic Intensity Grids and Magnetic Field Data Enhancements of the Merged Grids*, Data Package GDP00117_GCAS_MERGED_TMI_GRIDS_ERS. Department for Energy and Mining, South Australia, Adelaide.

Kelka U, Martínez C, Krapf CBE, Westerlund S, González-Álvarez I, Pawley MJ and Foss C 2022. Establishing an integrated workflow identifying and linking surface and subsurface lineaments for mineral exploration under cover: example from the Gawler Craton, South Australia. *Solid Earth* 13(4): 827–847. doi:10.5194/se-13-827-2022

Lourenco JS and Morrison HF 1973. Vector magnetic anomalies derived from measurements of a single component of the field. *Geophysics* 38: 359-368. doi:10.1038/s41467-020-19160-7

Miller HG and Singh V 1994. Potential Field Tilt a New Concept for Location of Potential Field Sources. *Journal of Applied Geophysics* 32, 213-217. doi:10.1016/0926-9851(94)90022-1

Milligan PR and Gunn PJ 1997. Enhancement and presentation of airborne geophysical data. *AGSO Journal of Australian Geology & Geophysics*. 17 (2), 63-75.

Monmonier M 2018. *How to Lie with Maps*. University of Chicago Press, Chicago.

Müller RD, Sdrolias M, Gaina C, and Roest WR 2008. Age, spreading rates and spreading symmetry of the world's ocean crust. *Geochem. Geophys. Geosyst.,* 9, Q04006, NOAA, NCEI, NGDC doi:10.1029/2007GC001743.

Nabigian MN 1984. Towards a three-dimensional automatic interpretation of potential field data. *Geophysics* 49:780–786. doi:10.1190/1.1441706

NOAA 2023. Magnetic Field Calculators [data service]. National Centers for Environmental Information, National Oceanic and Atmospheric Administration (NOAA), U.S. Department of Commerce. accessed 23 March 2023.

Pawley M, Irvine J, Melville A, Krapf C, Thiel S, Gonzalez-Alvarez I, Kelka U and Martinez C 2021. Automated lineament analysis of the Gairdner Dolerite dyke swarm of the Gawler Craton. *MESA Journal* 95: 30–40 Department for Energy and Mining, South Australia, Adelaide.

Pratt DA, White AS, Parfrey KL and McKenzie KB 2020. ModelVision User Guide Version 17.0. Tensor Research Pty Ltd.

Roest WR, Verhoef J and Pilkington M 1992. Magnetic interpretation using the 3-D analytic signal. *Geophysics* 57:116–125. doi:10.1190/1.1443174

Rajagopalan S and Milligan P 1994. Image enhancement of aeromagnetic data using automatic gain control. *Exploration Geophysics* 25: 173-178. doi:10.1071/EG994173

Salem A, Williams S, Fairhead D, Smith R and Ravat D 2008. Interpretation of magnetic data using tilt -angle derivatives. *Geophysics* 73: L1–L10. doi:10.1190/1.2799992

Thyng KM, Greene CA, Hetland RD, Zimmerle HM and DiMarco SF 2016. True colors of oceanography: Guidelines for effective and accurate colormap selection. *Oceanography* 29: 9–13. doi:10.5670/oceanog.2016.66 (Open Access)

Verduzco B, Fairhead JD, Green CM and MacKenzie C 2004. New insights into magnetic derivatives for structural mapping. *The Leading Edge* 23: 116–119. doi:10.1190/1.1651454

APPENDIX

GCAS TREND CONFIDENCE DATA PACKAGE

A GCAS Trend Confidence Data package (GPD000123) accompanies this report book and can be downloaded via the following link: http://dsd-gdp.s3.amazonaws.com/2043140/GDP00123.zip

Explanatory notes on the data package contents and how to use the contained data are included within the Zip file.